PEOPLE'S DEMOCRATIC REPUBLIC OF ALGERIA

MINISTRY OF HIGHER EDUCATION AND SCIENTIFIC RESEARCH

SETIF 1 UNIVERSITY - FERHAT ABBAS

FACULTY OF SCIENCES

DEPARTMENT OF PHYSICS



Setif 1 University - Ferhat ABBAS

# Evaluation of the Maxwellian Averaged Cross Section (MACS) at kT = 30 keV

By

**DJERBOUA Youcef**

Thesis Submitted to the Department of Physics

In Candidacy

For the degree of Doctorate LMD

In Subatomic Physics and Engineering

Defended on 14/11/2024 In front of the jury:

| | | |
|---|---|---|
| Dr. BOUKHENFOUF Wassila | University of Setif 1 - Ferhat Abbas | President |
| Prof. AMRANI Naima | University of Setif 1 - Ferhat Abbas | Supervisor |
| Dr. MASTINU Pierfrancesco | INFN-LNL, Legnaro (Padova), Italy | Co-Supervisor |
| Dr. YAKHELEF Abderrahmane | University of Setif 1 - Ferhat Abbas | Examiner |
| Dr. BENZAID Djelloul | University of Khemis Miliana | Examiner |
| Dr. BENTRIDI Salah-Eddine | University of Khemis Miliana | Invited Member |

# *Thanks*

*First of all, I thank my God for helping me achieve this goal, and for defying all obstacles in order to complete this thesis.*

*I would like to express my deepest gratitude to my thesis supervisor, **Mrs. Naima AMRANI**, professor at Sétif 1 University - Ferhat Abbes. She provided me with every opportunity necessary to conduct this work. Her availability, guidance, assistance, wise advice, and optimism were immensely valuable to me throughout this project, and it was a pleasure to work alongside her.*

*I would like to express my sincere gratitude to my thesis co-supervisor **Mr. Pierfrancesco MASTINU** first researcher and **Mrs. Elizabeth Musacchio-González** researcher, at Laboratori Nazionali di Legnaro INFN (Padova) Italy. Their availability, the clarity of their explanations, their patience, their determination, and the freedom they granted me have served as a particularly effective example and support during moments of uncertainty. They have also introduced me to the world of research.*

*I would also like to warmly thank the members of the Jury, **Dr. Abderrahmane YAKHELEF**, **Dr. Djelloul BENZAID** and **Dr. Salah-Eddine BENTRIDI**, who did me the honor of agreeing to judge this thesis work and for having read this manuscript carefully. I thank them for their interest in my work, for their remarks, for their questions and their discussions, as well as **Dr. Wassila BOUKHENFOUF** for having chaired my defense.*

*I would like to sincerely express my gratitude to **Mr. Ahmed BOUCENNA**, professor at Sétif 1 University - Ferhat Abbes. It was he who truly ignited my passion for subatomic physics engineering. His teaching, advice, attentive listening, and assistance, both scientifically and personally, have greatly contributed to my specialization in this field.*

*I would also like to thank all the people of the Department of Physics and Laboratori Nazionali di Legnaro INFN (Padova) Italy. May all those who have helped me from near and far during my training, find here my deepest thanks and my deepest gratitude.*

*Finally, I would like to express my sincere thanks to my family and all friends who encouraged and supported me to carry out this work.*

*                                                                                    **Thanks to all …***

# *Dedication*

*I dedicate this work; fruit of my years of study; as a sign of gratitude and respect, to the most loved ones:*

*To my dear mother for all her sacrifice and encouragement,*

*To my dear father for all that he gave me,*

*To my brother and sisters,*

*To all my teachers,*

*To all my family,*

*To all my friends,*

*To all who helped me from near or far,*

*Finally, to all those I have not mentioned and who are all so dear to me.*

*« Vision without action is merely a dream. Action without vision just passes the time. Vision with action can change the world »*

**Joel Arthur Barker**

*« The works of the mind, of science and of knowledge must serve humanity to make life simpler and more beautiful, and not to the enrichment of a few individuals »*

**Nikola Tesla (1856-1943)**

# *Summary*

# *Chapter 2*
# *Maxwellian Averaged Cross Section (MACS)*

# *Chapter 3*
# *Systematics of Maxwellian Averaged Neutron Capture Cross Sections (MACS) at 30 keV*

# General Introduction

# *General Introduction*

Nuclear data measurements and especially neutron induced cross sections take a particularly important place in human life and in many fields of applied nuclear physics, like those related to the application of new technologies for the production of nuclear energy and to the compilation of evaluated databases. Accurate knowledge of neutron-induced activation cross sections is of great interest to many fields of nuclear science.

In the nuclear field, the precise neutron capture cross section in the energy range of 1 keV - 2 MeV are required for the reliable processing of transmutation of nuclear waste and for the design of next generation fission reactors (Gen IV and thorium base cycle).

In the field of astrophysics, the largest amount for calculating the ratio of stellar reactions is the Maxwellian Averaged Cross Section (MACS).

Also the (n,γ) cross section values are irreplaceable tools for developing nuclear reaction theories by means of nuclear models validation. Neutron capture reactions in the energy range 1-600 keV are the basic mechanism to explain the formation of the elements heavier than iron during stellar nucleosyntethis. Accordingly, the Maxwellian Averaged Cross Sections (MACS) are the key ingredient for calculating the reaction rates inside the stars and thus for reproducing the observed abundances of the elements in the Universe.

Unfortunately, the analysis of existing databases shows problems of incompleteness and large discrepancies among available nuclear data. Obviously, the possibility of obtaining reliable measurements of requested nuclear data depends on corresponding neutron facilities performances [1]. However, it is essential to produce complementary neutron-induced reaction data sets for an independent verification and to expand the boundaries of the data tables [2].

The calculation of the cross sections of nuclear reactions makes an important contribution to the study of nuclear interaction, the nuclear structure and the reaction mechanism. For the determination of the cross sections which cannot be measured experimentally, we have recourse to a faster and more flexible alternative calculation based on systematic studies worked out on the basis of experimental data and simple theoretical models proves more useful and allows faster determination of cross sections, which can be extrapolated to cases where measurements are almost impossible. That has led experimenters and theorists to develop theoretical methods and models. Experimental data represents a test to verify the consistency and validity of nuclear models, designed for the analysis of nuclear interactions. These theoretical models, in turn, fill the void in data that is not accessible to experience. The combination of the two theoretical and experimental approaches also leads to systematic studies for reliable and rapid assessments of nuclear data [3-12].

For the experimental part and for many reasons like first negative results obtained and lockdown related to the Covid-19 pandemic, we limited our work to theoretical part.

The objective of this thesis work is to derive a formula for calculating the Maxwellian averaged neutron capture cross sections (MACS) at energy of kT = 30 keV. This study is conducted for 89 isotopes for 15 elements with mass numbers ranging from 70 to 204. The experimental data utilized in this study are extracted from the KADoNiS database. The calculated values of the cross sections obtained using the new formula are compared with the experimental values.

This thesis is subdivided into three chapters:

The first chapter serves as a theoretical recapitulation, providing a comprehensive exposition of fundamental principles concerning the atomic nucleus, nuclear reaction with interactions involving neutrons and matter, nuclear reaction models, radiative capture reaction (n, γ), and cross section.

In the second chapter, we delve into the Maxwellian Averaged Cross Section (MACS) concept, as well as how to generate the neutron spectrum through the $^7$Li (p, n) $^7$Be reaction in an accelerator (VDG) who will contributed to calculate MACS for elements, and how measuring the Maxwellian Averaged Cross Section (MACS) at kT= 30 keV by Activation.

In the third chapter, a Maxwellian averaged neutron capture cross sections (MACS) formula is derived for target nuclei with mass number A $\gg$ 1 and 30 keV incident neutron energie. A detailed discussion is introduced for results.

# Chapter 1

# Nucleus and nuclear reaction

# *Chapter 1*

# *Nucleus and nuclear reaction*

**I. Atomic nucleus**

**1. Definition**

The atomic nucleus is the heart of the atom. It is located in its center, but a thousand times smaller and contains 99.97% of its mass. The nucleus contains nucleons, i.e. protons and neutrons and a positive electric charge. The cohesion of the atomic nucleus is ensured by the strong interaction, which attracts the nucleons together and thus prevents the protons from repelling each other. The size of the nuclei is of the order of $10^{-15}$ m or 1 fermi. The nucleus is composed of A nucleons, including Z protons and (A-Z) neutrons. The nucleus X will be noted as follows: $_Z^A\mathbf{X}$ [13].

**2. Mass Defect**

The mass defect **Δm** of a nucleus with symbol $_Z^A\mathbf{X}$ is the difference between the mass of its isolated nucleons at rest and the mass of the nucleus at rest [14].

$$\mathbf{\Delta m = (Z \times m_p + (A - Z) \times m_n) - m_{nucleus}} \tag{1-1}$$

With :

**m$_p$**: mass of the proton

**m$_n$**: mass of the neutron

**m$_{nucleus}$**: mass of the nucleus

The mass defect is conventionally always strictly positive because the mass of a nucleus is always less than the sum of the masses of its constituent nucleons [14].

## 3. Binding energy

The binding energy of a nucleus, denoted ($E_l$), is the energy needed to dissociate this nucleus at rest into its free nucleons at rest. The binding energy of a nucleus is related to its mass defect [14].

$$E_l = \Delta m \times c^2 \tag{1-2}$$

With :

$E_l$: binding energy (J)

$\Delta m$: mass defect (kg)

c: speed of light in a vacuum (m/s) (c = 299792458 m/s)

## 4. Binding Energy per Nucleon

The binding energy per nucleon $E_A$ (generally expressed in MeV/nucleon) is the value of the binding energy $E_l$ divided by the mass number **A** of the nucleus [14].

$$E_A = \frac{E_l}{A} \tag{1-3}$$

The binding energy per nucleon is an index of the stability of the assembly of nucleons that forms the nucleus: the greater the binding energy per nucleon, the more bound the nucleus is (***Figure 1.1***) [14].
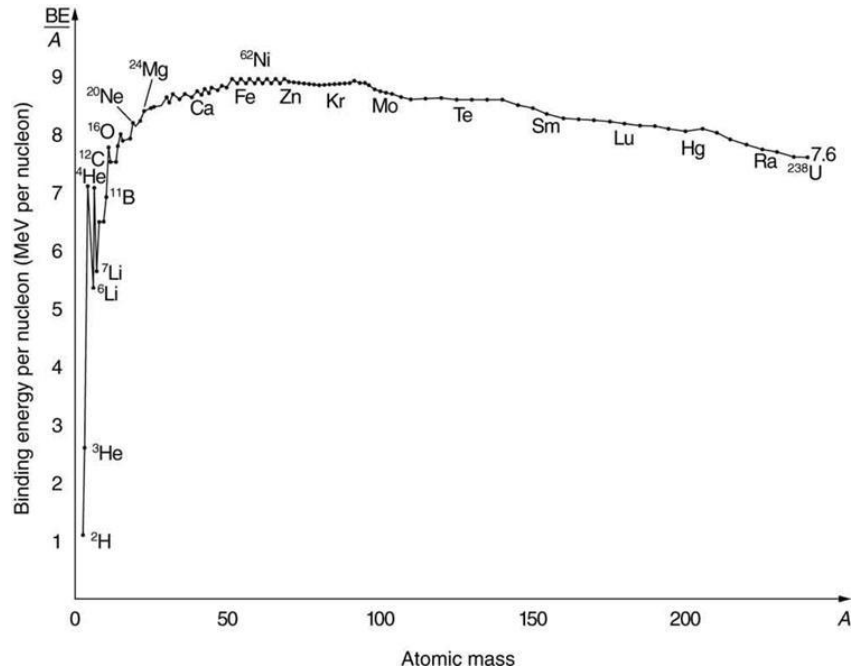
**Figure 1.1.** Binding energy per nucleon as a function of mass number [13].

From this figure, we can observe that the most stable nuclei have a higher binding energy per nucleon [14].

**5. Formule semi-empirique de masse**

The ***nuclear model of the liquid drop*** leads to the semi-empirical ***Bethe-Weizsäcker*** formula for the binding energy [14].

$$\textbf{B(Z; A)} = \textbf{a}_v\textbf{A} \ - \textbf{a}_s\,\textbf{A}^{2/3} \text{-} \textbf{a}_c\,\frac{Z(Z-1)}{A^{1/3}} - \textbf{a}_a\,\frac{(A-2Z)^2}{A} \pm \delta\textbf{(Z, N)} \qquad \textbf{(1-4)}$$

The physical meaning of the five parameters of the formula and their values are as follows, *Figure 1.2* [14]:

$$\textbf{a}_v = \textbf{15.56 MeV} : \text{volume parameter}$$

$$\textbf{a}_s = \textbf{17.23 MeV} : \text{surface parameter}$$

$$a_c = 0.72 \text{ MeV} : \text{Coulomb parameter}$$

$$a_a = 23.6 \text{ MeV} : \text{asymmetry parameter}$$

$$\delta(Z, N) = a_p A^{-1/2} : \text{pair parameter}$$

$$\text{Where } a_p = \begin{cases} -11 \text{ MeV} & \text{for Z and N odd} \\ 0 & \text{for A odd} \\ 11 \text{ MeV} & \text{for Z and N even} \end{cases}$$
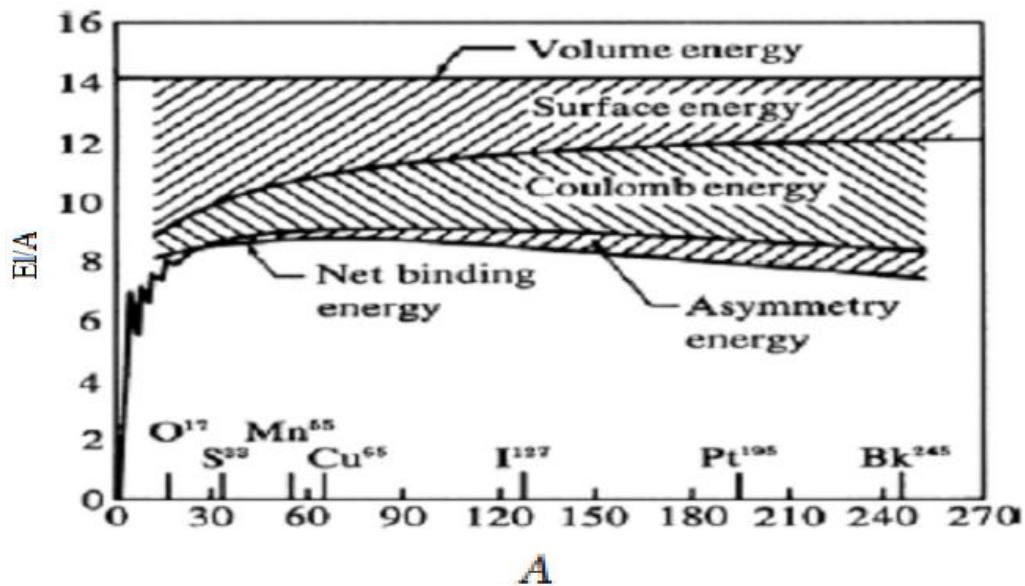


**Figure 1.2.** Contribution of each term in the Bethe-Weizsäcker formula for the binding energy per nucleon, in MeV, as a function of mass number A [14].

## 6. Nuclei Stability

Not all nuclei are stable. Unstable nuclei undergo radioactive decay and transform into other stable or less radioactive nuclei. Stable nuclei have approximately equal numbers of neutrons and protons, N = Z, in the case of light nuclei. However, for heavy nuclei, there is a smaller difference between the number of neutrons and protons, as illustrated in *Figure 1.3* [15].
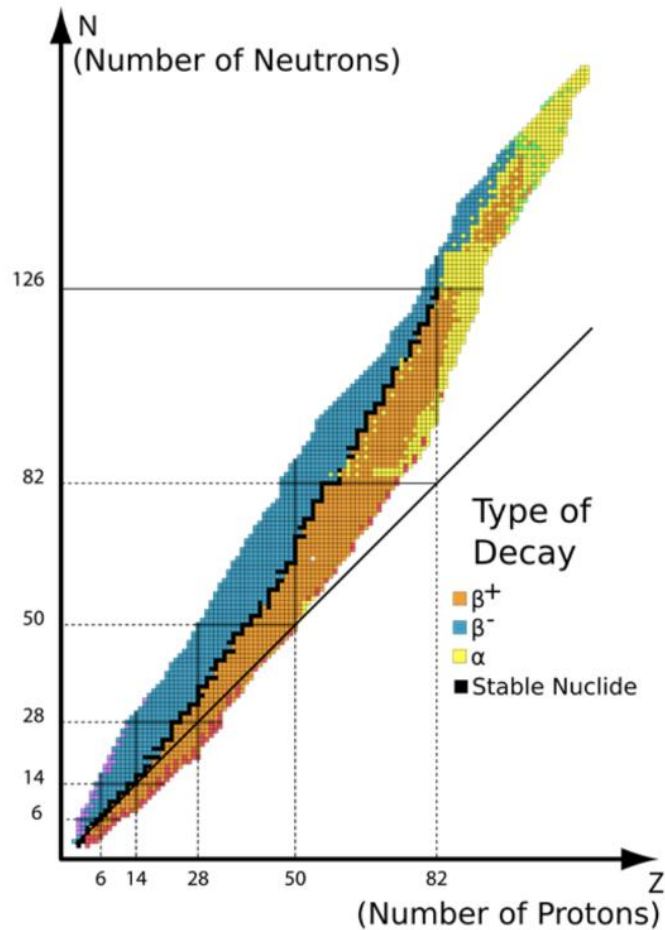
**Figure 1.3.** Stability chart [13].

Unstable nuclei undergo series of radioactive decays until they become stable [16]:

In the central black region, we find stable nuclei.

Above the stable nuclei, in blue, we find nuclei that are neutron-rich. These nuclei move towards the stability line through **β⁻ decay**. Conversely, below the stable nuclei, in orange, we find nuclei that are proton-rich. These nuclei move towards the stability line through **β⁺ decay** or **electron capture**.

Heavy nuclei, in yellow, return to the stability line through **alpha decay** [17].

## 7. Radioactivity

In 1896, Henri Becquerel discovered that uranium and its compounds continuously emit radiation. Pierre and Marie Curie, continuing Becquerel's work, gave this phenomenon the name *radioactivity* [18].

### 7.1. Different Modes of Decay

*α Decay* corresponds to the emission of a helium nucleus ($_2^4$He) by certain nuclei. This type of radioactivity occurs in nuclei that have an excess of nucleons (neutrons and protons) and are referred to as "heavy nuclei" (A > 200). In this transformation, the atomic number Z decreases by two units, and the mass number A decreases by four units.

The general equation for alpha decay is as follows [19]:

$$_Z^A X \rightarrow \, _{Z-2}^{A-4} Y + \, _2^4 He$$
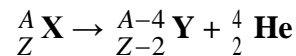
*β⁻ Decay* corresponds to the emission of an electron and an antineutrino by certain nuclei. This type of radioactivity is observed in nuclei with an excess of neutrons. During this transformation, the atomic number Z increases by one unit while the mass number A remains conserved.

The general equation for beta minus (β⁻) decay is as follows [19]:

$$_0^1 n \rightarrow \, _1^1 p + e^- + \bar{\nu}$$

$$_Z^A X \rightarrow \, _{Z+1}^A Y + e^- + \bar{\nu}$$
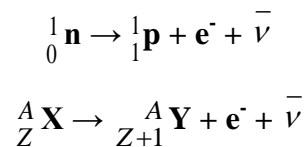
*β⁺ Decay* corresponds to the emission of a positron (or positrons) and a neutrino by certain nuclei. This type of radioactivity is observed in nuclei with an excess of protons. During this transformation, the atomic number Z decreases by one unit while the mass number A remains conserved.

The general equation for beta plus ($\beta^+$) decay is as follows [19]:

$$\ce{^1_1 p} \rightarrow \ce{^1_0 n} + e^+ + \nu$$

$$\ce{^A_Z X} \rightarrow \ce{^A_{Z-1} Y} + e^+ + \nu$$
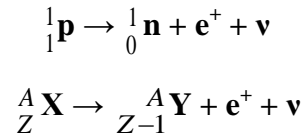
**Note:** The mass of a neutrino and an antineutrino (if any) is extremely small and can be considered approximately zero [14].

***Electron capture*** (denoted as E.C.) corresponds to the absorption of an electron from the electron cloud by a proton. During this transformation, the atomic number Z decreases by one unit, and the mass number A is conserved without the emission of a positron [14].

The general equation for electron capture (E.C.) decay is as follows [19]:

$$\ce{^1_1 p} + e^- \rightarrow \ce{^1_0 n} + \nu$$

$$\ce{^A_Z X} + e^- \rightarrow \ce{^A_{Z-1} Y} + \nu$$
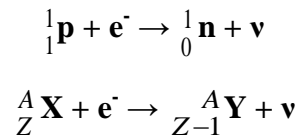
If the daughter nucleus resulting from radioactive decay α or β is in an excited state, the excess energy is released in the form of high-frequency electromagnetic radiation γ. This phenomenon is referred to as ***de-excitation γ***. A nucleus in an excited state is denoted with an asterisk as a superscript on the right.

The general equation for gamma (γ) de-excitation is as follows [19]:

$$\ce{^A_Z X}^* \rightarrow \ce{^A_Z X} + \gamma$$
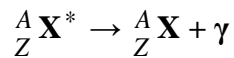
### 7.2. Laws of Decay

The fundamental law of radioactive decay states that the rate of transformation of a nucleus ensemble is proportional to the number of nuclei present at time t=0, denoted as **$N_0$** [16]. The radioactive decay law at time t is given as follows [14]:

$$\mathbf{N(t)= N_0e^{-\lambda t}} \tag{1-5}$$

Where:

**N(t)**: the number of nuclei that will decrease over time

**$N_0$**: the initial number of nuclei present

λ: the radioactive decay constant, which depends on the nature of the radioactive nucleus. It represents the proportion of nuclei that decay per unit of time ($s^{-1}$) [14].

The *activity* of a sample is the number of decays per unit of time, denoted as A(t). It can be calculated simply [16]:

$$\mathbf{A(t) = \lambda N(t) = \lambda N_0e^{-\lambda t} = A_0e^{-\lambda t}} \tag{1-6}$$

Where:

**A(t)**: the activity

**$A_0$**: ($\lambda \times N_0$) the initial activity [19].

The measurement of radioactivity intensity (activity) is carried out using the following two units:

***The Becquerel***, symbol Bq, represents one decay per second.

$$1 \text{ Bq} = 1 \text{ decay/second}$$

***The Curie***, symbol Ci, is an older unit that is less commonly used.

$$1 \text{ Ci} = 3{,}7 \times 10^{10} \text{ decays/second}$$

This corresponds to the activity of 1 g of $^{226}$Ra with a half-life of T = 1620 years [14].

$$\mathbf{T=}\frac{\ln 2}{\lambda} \qquad\qquad \textbf{(1-7)}$$

Where:

**T**: half-life, is the time at which the initially present number of nuclei will be divided by two (s) [19].

**II. Nuclear reaction**

**1. Definitions**

In the field of nuclear physics, a nuclear reaction is a phenomenon whereby two atomic nuclei or nuclear particles collide, resulting in the formation of distinct products that differ from the initial particles [20]. The objective of nuclear reactions is to investigate nuclear structures and the properties of interactions. [21].

In principle, a nuclear reaction can involve more than two particles colliding. However, due to the significantly lower probability of three or more nuclei simultaneously meeting at the same location, such an event is exceptionally rare [20].

If the projectile is a charged particle (protons, deuterons, tritons, alpha particles, etc.), the electric repulsion experienced from the charge of the target nucleus tends to deflect it and prevent it from reaching the nucleus. Photons, which are uncharged, constitute an electromagnetic radiation, that's why their interactions have low efficiency. The preferred projectile is the neutron, which is not deflected by the electric field of the target due to its lack of charge. Additionally, at low velocity, the neutron lingers for a longer time near the nucleus, making it more prone to easily interact with it.

When a target nucleus **X** is bombarded by an incident particle **a**. The result of the interaction is an ejected particle **b** and a recoiling nucleus **Y**, *Figure 1.4* [22].

$$a + X \rightarrow b + Y$$
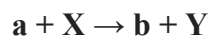
Abbreviated: **X (a, b) Y**

Where ;     **a** : incident particle (projectile particle)

$\qquad$ **X** : target nucleus

$\qquad$ **b** : particle produced

$\qquad$ **Y** : residual nucleus (recoil nucleus)
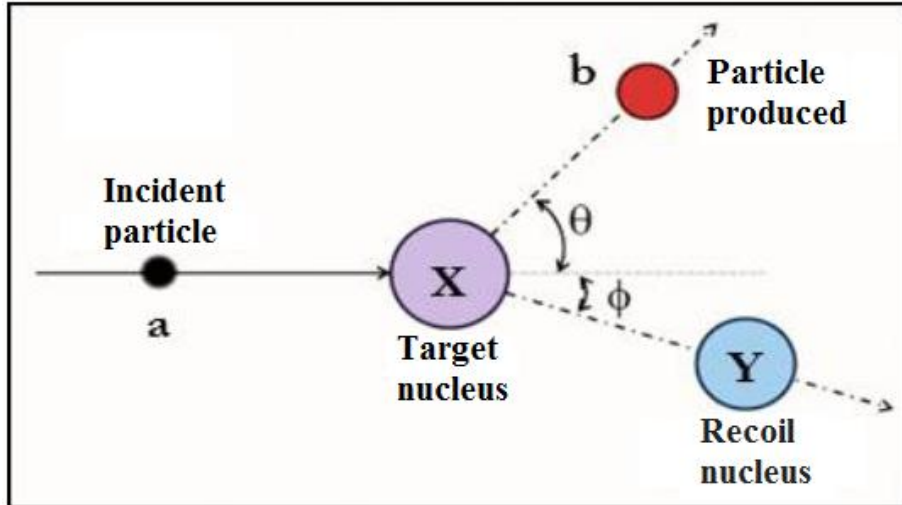
**Figure 1.4.** Schematic representation of a nuclear reaction [22].

## 2. Characteristics of a nuclear reaction

The particles involved in a nuclear reaction constitute an isolated system. The following quantities, pertaining to this system, form the ***conservation laws*** during the reaction as follows [18] :

      • The number of nucleons, A.

      • The electric charge and the charge number, Z.

      • The sum of kinetic energy, $E_c$, and rest energy, $E_o$, before and after the reaction.

      • The momentum, $\overrightarrow{P}$.

The ***energy balance*** of a nuclear reaction, denoted as **Q**, is the difference between the kinetic energy of the reaction products and the initial kinetic energy [23].

Consider the following nuclear reaction [14]:

$$a + X \rightarrow b + Y$$
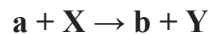
The energy balance of the interaction is defined as:

$$Q = T_f - T_i \tag{1-8}$$

$T_f$ and $T_i$ represent the kinetic energies after and before the interaction, respectively.

$$T_f = T_b + T_y \quad \text{and} \quad T_i = T_a + T_x \tag{1-9}$$

$$Q = T_b + T_y - T_a \tag{1-10}$$

$$Q = [M_a + M_x - M_b - M_y] \, C^2 \tag{1-11}$$

$M_a$, $M_x$, $M_b$ and $M_y$ represent the atomic masses of the reactive particles and reaction products, respectively.

Three cases can occur [14]:

- If $Q > 0$, the reaction is exoenergetic:

    For the Uranium fission reaction, the energy balance is $Q = 200$ MeV.

    For the vast majority of nuclear reactions the $Q < 10$ MeV.

- If $Q = 0$, it's a phenomenon of elastic scattering, where the internal state of the system's constituents remains unaltered.

    - If $Q < 0$, the reaction is endoenergetic. This type of reaction only occurs if the incident particle possesses energy $\geq |Q|$.

## 3. Type of nuclear reactions

Nuclear reactions involve various mechanisms of interaction. As the projectile approaches a target nucleus, it has a certain probability of interacting with the average nuclear field. Three reaction mechanisms can be distinguished as a result of this interaction [24]:

• The *elastic scattering* reaction, also known as "shape elastic" reaction, corresponds to the deviation of the projectile's trajectory by the nuclear potential, without any energy loss. There is no energy sharing between the projectile and the nucleons of the target nucleus.

$$a + X \rightarrow X + a.$$
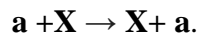
• ***Direct reactions*** are characterized by their rapidity (on the order of the time it takes for the projectile to traverse the nucleus, approximately $10^{-22}$s) and involve minimal interactions between the projectile and the nucleons at the periphery of the nucleus.

• Reactions leading to the formation of a ***compound nucleus*** (CN) represent a more complex scenario in which the incident particle is captured by the target due to strong interaction, sharing its energy with all nucleons of the target nucleus. The characteristic timescale of this reaction mechanism is on the order of $10^{-17}$s. For incident neutron energies in the range of several tens of MeV, the nucleus may undergo an intermediate state known as pre-equilibrium, during which particle emission can occur prior to the formation of a compound nucleus, as depicted in ***Figure 1.5***.

$$a + X \rightarrow Y *, Y* \rightarrow c + d.$$
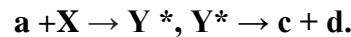
All these mechanisms can generate several types of nuclear reactions: elastic, inelastic diffusion, capture reactions, fission and many others [24].
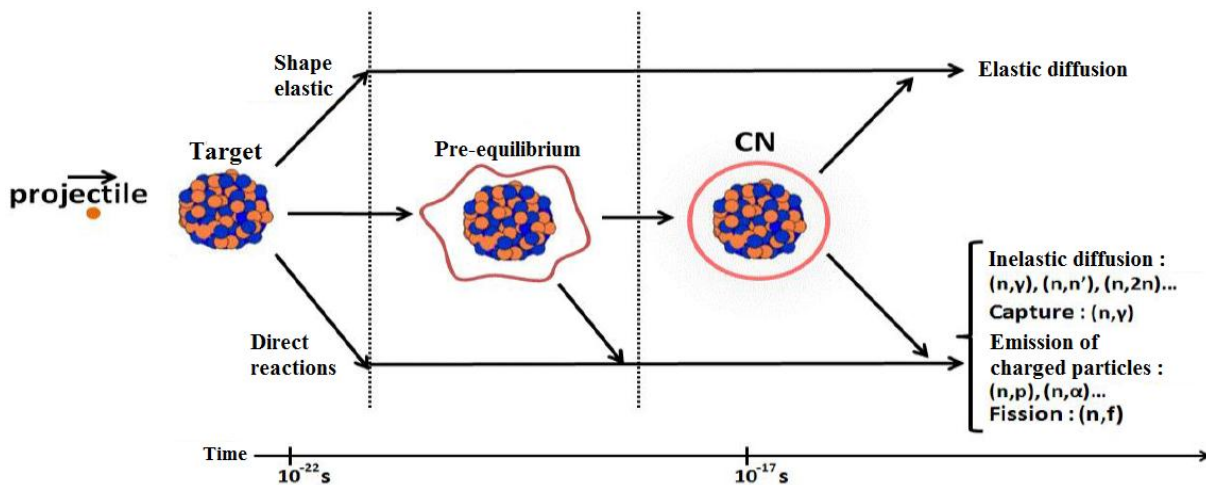


**Figure 1.5.** The different mechanisms of nuclear reactions [24].

## 4. Neutron-induced reactions

A neutron-induced nuclear reaction is a process in which a neutron interacts with a nucleus, resulting in the emission of two or more particles. Sometimes, when a nucleus interacts with

another nucleus or particle without changing the nature of the nuclide, the process is referred to as nuclear scattering rather than a neutron-induced nuclear reaction [13]. Neutron scattering can be elastic or inelastic. The neutron-induced nuclear reaction can cause a transformation of the target nuclide into another nuclide by absorbing the incident neutron [25].

**4.1. Neutrons**

The neutron is a particle that carries no electric charge, making it suitable for bombarding atoms and reaching their nuclei. It has a mass close to, but slightly greater than, that of a proton. Outside the nucleus, the neutron is free and has an average lifetime of 15 minutes. It undergoes a decay process into a proton, an electron, and an antineutrino. The equation for neutron decay is given by [25]:

$$\mathbf{n \rightarrow p + e + \bar{\nu} + 0,78\ MeV}$$
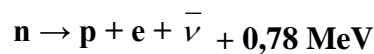
The physical properties of the neutron are provided in ***Table 1.1***[25].

| Mass | $m_n = 1,675 \times 10^{-27}\ Kg$ |
|---|---|
| Electric charge | $q_n = 0$ |
| Size | $r_n \sim 1\ Fermi$ |
| Internal structure: quarks | ddu |
| Spin | $s_n = \frac{1}{2}$ |
| Magnetic dipole moment | $\mu_n / \mu_p = -0,68497935$ |
| Electric dipole moment | 0 |

**Table 1.1.** Properties of the neutron [25].

A large number of nuclear reactions produce beams of neutrons. Unlike charged particles, neutrons cannot be accelerated directly, but they can be slowed down through successive collisions with carefully selected nuclei. This process of slowing down is called moderation, and

the nuclei that serve as "slowing down" agents are referred to as moderators [26]. Neutrons can be classified based on their energy, as shown in ***Table 1.2*** [27]:

| Classification | Energy |
|---|---|
| Thermal neutrons | $E_n = 0,025$ eV |
| Epi-thermal neutrons | $0,5$ eV $< E_n < 1$ keV |
| Intermediate neutrons | $1$ keV $< E_n < 500$ keV |
| Fast neutrons | $0,5$ MeV $< E_n < 20$ MeV |
| Ultra Fast Neutrons | $20$ MeV $< E_n < 50$ MeV |
| Relativistic neutrons | $E_n > 50$ MeV |

**Table 1.2.** Classification of neutrons based on their energy [27].

### 4.2. Neutron Sources

Neutrons can be produced through various methods, including radioactive sources, charged particle accelerators, or in nuclear reactors through the fission process.

### a. Radioactive sources

The emission of neutrons occurs as a result of the ***Spontaneous fission*** of certain heavy elements that decay through fission at a specific rate, on average emitting 2.5 neutrons per fission. Among these elements, **Californium-252** ($^{252}$Cf) (with a half-life of 2.645 years) is particularly noteworthy [28]. Its decay through alpha emission (with a probability of 96.91%) and spontaneous fission (with a probability of 3.09%) results in a neutron emission rate of $2,314 \times 10^6$ neutrons.s$^{-1}$.µg$^{-1}$ [29].

***Neutron sources based on induced reactions*** typically include sources utilizing (α, n), (γ, n), (p, n) and (d, n) reactions.

***Alpha-neutron (α, n) sources*** are composed of a homogeneous mixture containing an alpha-emitting isotope (in the form of a radioactive powder) and a light element (such as beryllium, boron, or lithium powder). The system can be described by the following equation [28]:

18

$$\ _2^4\alpha + \ _Z^A X \rightarrow [\ _{Z+2}^{A+4}Y]^* \rightarrow \ _{Z+2}^{A+3}Y + \ _0^1n$$
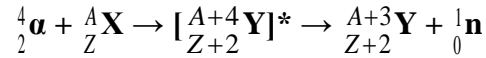
From this reaction, a fast neutron is expelled, leaving the nucleus Y in a stable state. In the case where the light nucleus is beryllium, the reaction becomes [30]:

$$\ _2^4\alpha + \ _4^9 Be \rightarrow [\ _6^{13}C]^* \rightarrow \ _6^{12}C + \ _0^1n$$
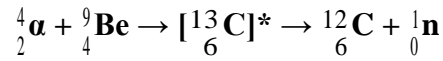
(α, n) sources are the most commonly used due to their high yield. The neutron flux produced is on the order of $10^6$ n/cm$^2$.s with an average energy of 4.5 MeV. The main (α, n) sources used include Pu-Be, Am-Be, and Ra-Be, as shown in ***Table 1.3*** [31].

| Source | Average Neutron Energy (MeV) | T (α particle half-life) |
|:---:|:---:|:---:|
| $^{210}$PoBe | 4.2 | 138 d |
| $^{210}$PoB | 2.5 | 138 d |
| $^{226}$RaBe | 3.9 | 1600 y |
| $^{226}$RaB | 3.0 | 1600 y |
| $^{239}$PuBe | 4.5 | 24100 y |

**Table 1.3.** Neutron Sources (α, n) [31].

Neutrons can also be produced through **(γ, n) reactions** by combining a γ-emitting radionuclide (γ photons serve as projectiles) with an appropriate target material. Photo-neutrons are obtained when the photon energy exceeds the neutron separation energy of the target nucleus. This energy is 1.67 MeV for $^9$Be, 2.23 MeV for $^2$H, and greater than 6 MeV for other nuclei. However, only Beryllium and Deuterium targets are used since there are no radionuclides that produce photons with energies exceeding 6 MeV. The corresponding reaction can be written as [31]:

$$\gamma + \ _Z^A Y \rightarrow [\ _Z^A Y]^* \rightarrow \ _Z^{A-1}Y + \ _0^1n$$
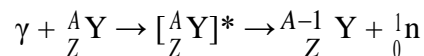
Most of these sources are based on the reactions $^9$Be ($\gamma$, n) $^8$Be and $^2$H ($\gamma$, n) $^1$H. The yield is on the order of $10^4$ neutrons per curie per second [31].

The significance of such sources lies in their compactness and low cost, as they produce mono-energetic neutrons. This is not the case with ($\alpha$, n) sources, which are used for calibrating fast neutron detectors [22]. Their main drawback lies in the necessity of using substantial shielding against gamma radiation [30].

**b. Particle accelerators**

Indeed, these installations accelerate charged particles and direct them towards target materials. The interaction of the incident particles with the nuclei of the target leads to the creation of new particles. By selecting appropriate targets and projectiles, the ejected particles can be neutrons. The nuclear reactions that can be used to produce neutrons are summarized in *Table 1.4* [32].

| Reaction | Target | Particle | Neutron energy (MeV) | Fast neutron flux (n/cm$^2$.s) |
|:---:|:---:|:---:|:---:|:---:|
| **T (d, n)** | Tritium | Deuterium | 2 to 4 | 1 to 4. $10^{11}$ |
| **Be (d, n)** | Beryllium | Deuterium | 4 | $10^{10}$ |
| **Be ($\gamma$, n)** | Beryllium | Gamma | 1,4 | 2. $10^{11}$ |

**Table 1.4.** Nuclear reactions used in accelerators for neutron production [32].

**c. Nuclear Reactors**

Nuclear reactors are extremely intense sources of neutrons. A nuclear reactor consists of an active core that contains fissile elements such as Uranium dispersed in a moderator medium, such as water, inside a reactor vessel. The entire system is contained within concrete structures, which also serve as biological shielding. A nuclear reactor has control mechanisms and a cooling system to regulate its power. Neutrons are produced by the induced fission of $^{235}$U, $^{238}$U, or $^{239}$Pu. In the case of $^{235}$U, fission occurs when a nucleus of $^{235}$U absorbs a thermal neutron [33].

## 4.3. Neutron-Matter Interaction

The interaction of ***neutrons with electrons*** is negligible due to the small size of an electron compared to the nucleus, and furthermore, the interaction can only be electro-weak and has a highly negligible cross-section compared to the cross-section of the interaction with the nucleus.

The ***neutron-neutron*** interaction is also negligible due to the neutron density, which is on the order of $10^{38}$ n/cm$^3$, resulting in a probability of one in $10^{14}$ for it to occur compared to the neutron-nucleus interaction. The primary form of interaction is scattering [34].

Neutrons are electrically neutral particles and are not sensitive to interactions with atomic electrons. Consequently, they traverse the electron cloud of an atom and interact directly with the nucleus, known as ***neutron-nucleus*** interaction [35].

In a material medium, neutrons undergo two types of phenomena: ***scattering***, in which the neutron loses energy and changes direction, and ***absorption***, a process in which the neutron disappears and gives rise to one or more particles. The most common absorption reaction is radiative capture [36].

## a. Diffusion reaction

The diffusion reaction occurs when a neutron collides with a stationary nucleus. The nucleus emits a single neutron, which may differ from the incident neutron.

> ➢ **Elastic scattering** *(n, n)*

In an elastic scattering reaction between the neutron and the target nucleus, the target nucleus remains in its ground state. This type of scattering plays a significant role in neutron slowing down within reactors, as depicted in ***Figure 1.6*** [37].
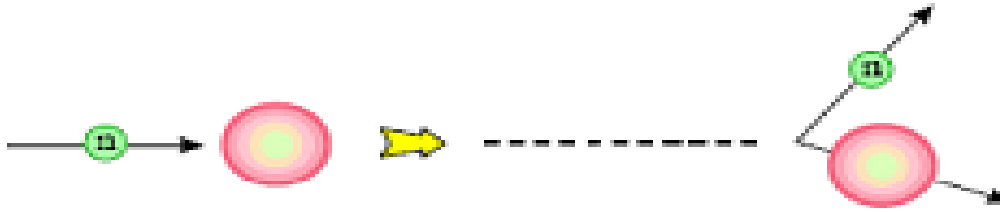
**Figure 1.6.** Elastic scattering of a neutron-nucleus [34].

Elastic scattering can occur in two ways:

- **Elastic potential scattering**

In this process, a neutron strikes a nucleus and transfers a portion of its energy to the nucleus. The neutron then rebounds in a different direction, while a recoil nucleus is produced.

- **Resonant elastic scattering**

In this process, a compound nucleus (neutron + nucleus) is formed. Subsequently, a neutron is reemitted by the compound nucleus with the same kinetic energy as the absorbed neutron.

➢ **Inelastic scattering** *(n, n')*

In inelastic scattering, the incident neutron is captured, forming a compound nucleus. Subsequently, a neutron is reemitted, but with lower kinetic energy compared to elastic scattering. The residual nucleus is left in an excited state and emits gamma radiation to return to its ground state, as illustrated in *Figure 1.7* [37].
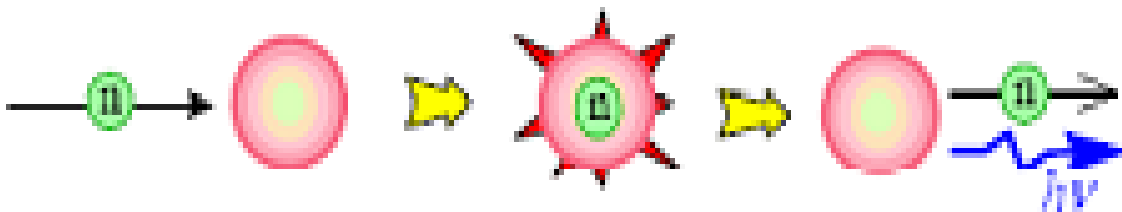


**Figure 1.7.** Inelastic scattering of a neutron-nucleus [34].

**b. Absorption reaction**

&#10149; **Radiative capture**

In this process, the neutron is captured by the nucleus, forming a compound nucleus with a mass number (A+1) in an excited state. The compound nucleus subsequently de-excites by emitting one or more gamma radiations. This interaction is exoenergetic and denoted as (n, γ), as shown in *Figure 1.8*. This mechanism is particularly significant for thermal neutrons. Certain materials, such as Cadmium and Boron, exhibit highly significant capture cross-sections and are employed for control and shutdown of nuclear reactors [37].
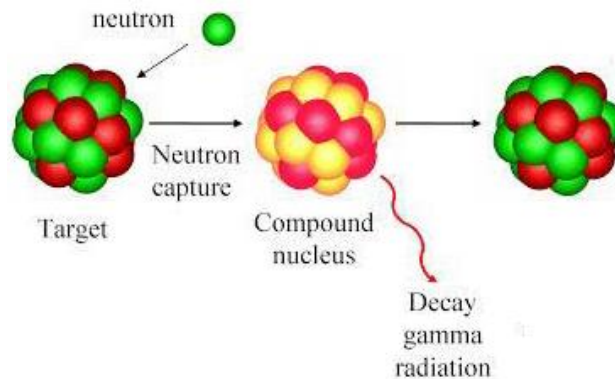


**Figure 1.8.** Radiative capture reaction [37].

&#10149; **Nuclear reactions (n, x)**

Neutrons can also disappear through absorption reactions such as (n, α) and (n, p), as shown in *Figure 1.9*. These reactions can be either exoenergetic or endoenergetic [37].
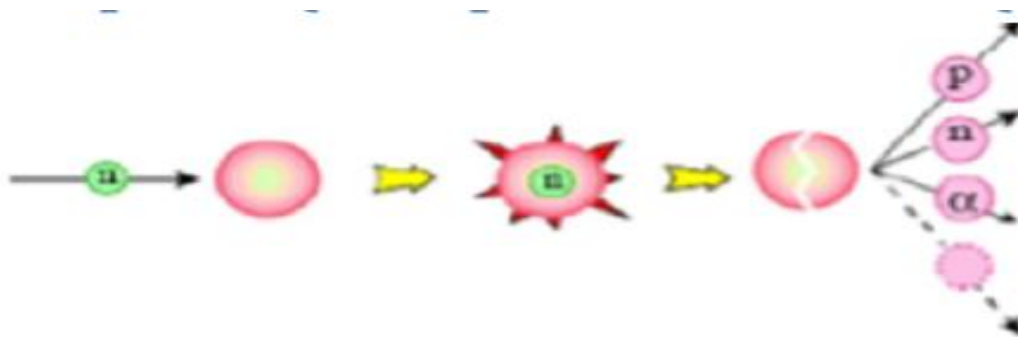


**Figure 1.9.** Neutron absorption reaction [34].

➤ **Nuclear reactions (n, xn) with** x=2.3…

Reactions of the type (n, 2n) and (n, 3n) occur with energetic neutrons. It's clear that these reactions are endoenergetic since in the (n, 2n) reaction, one neutron, and in the (n, 3n) reaction, two neutrons are ejected from the target nucleus.

➤ **Fission reactions (n, f)**

Neutrons colliding with certain nuclei can induce the nucleus to undergo fission, which is the process of splitting. These reactions primarily involve heavy elements such as Th, U, Np, and Pu. After interacting with these actinides, the neutrons result in the formation of a compound nucleus that subsequently splits into two fragments along with the emission of one or more fast neutrons and the release of energy, as shown in ***Figure 1.10*** [37].
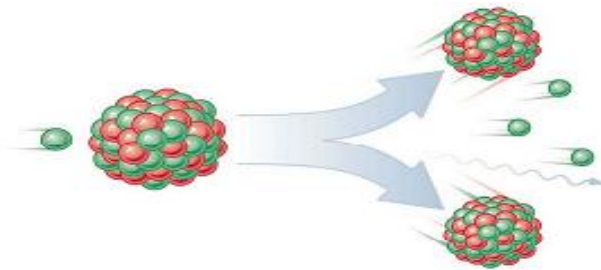


**Figure 1.10.** Fission reaction [34].

***Figure 1.11*** illustrates the different types of reactions induced by neutrons [38].
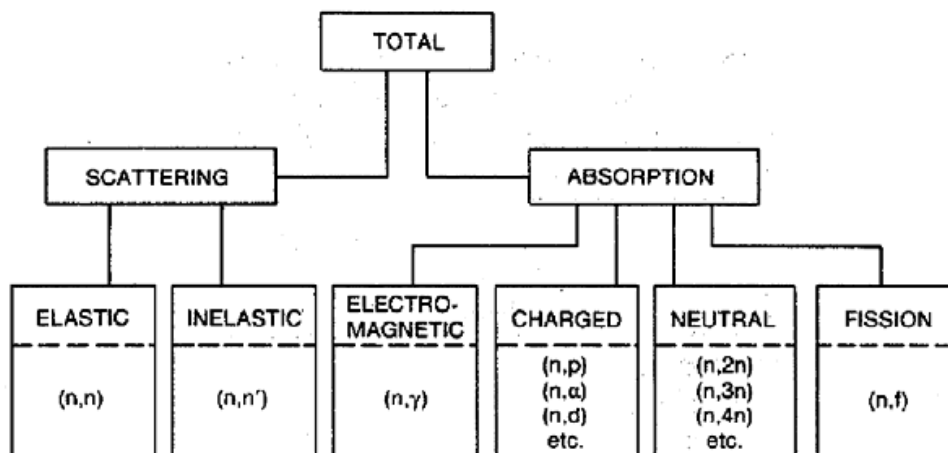


**Figure 1.11.** The different categories of neutron interactions [38].

## III. Nuclear reaction models

There are several possible outcomes for neutron-induced nuclear reactions [39]. The probabilities of these reactions occurring (cross-sections) depend on the nature and energy of the projectile (neutron). Modeling nuclear reactions remains a complex task that requires a substantial amount of information and experimental data to enhance our theoretical understanding, as depicted in ***Figure 1.12*** [40].
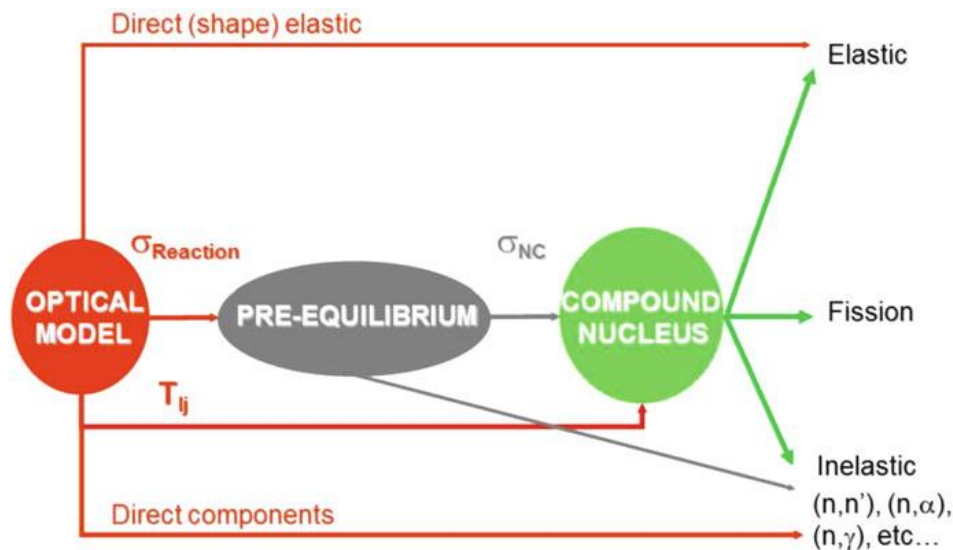


**Figure 1.12.** Nuclear reaction models [40].

## 1. The optical model

The optical model is an approach to ***nucleon-nucleus*** scattering in which the incident nucleon interacts with a complex potential that represents its interaction with all the nucleons constituting the target nucleus. Since nucleon scattering on a nucleus occurs at the subatomic scale, quantum mechanics governs this phenomenon. The projectile nucleon is described as a wave function. This wave, refracted by the potential representing the target nucleus, interferes with the incident wave [40].

## 2. The pre-equilibrium model

The process of pre-equilibrium is named as such because the emission of a particle during a nuclear reaction takes place before the equilibrium of the compound nucleus is established. When a neutron collides with a nucleus, before reaching the final state of the reaction and before the equilibrium process is achieved, a two-body interaction process is triggered. This leads to the creation of a particle-hole pair that further interacts (particle-particle and hole-hole) with other nucleons in the nucleus, creating a new particle-hole pair at each interaction, until equilibrium is reached. During this series of interactions, a nucleon (proton or neutron), a cluster of nucleons (nn, np, nnp, ppn, etc.), or an alpha particle can be emitted. This phenomenon is referred to as pre-equilibrium particle emission [34].

## 3. The compound nucleus model

In the ***compound nucleus*** formation reaction model, the nuclear projectile approaches the target nucleus and undergoes strong interactions with all nucleons in the nucleus. The incident kinetic energy (which is low) is rapidly distributed among all nucleons of the composite nucleus, formed by the initial nucleus and the projectile nucleus.

The composite nucleus is in an ***excited state***, leading to the second stage of the nuclear reaction: the emission of one or several light particles (n, p, γ, t, α, ...). It undergoes decay independently of its formation mode (the interactions involved in its formation are so complex and numerous that it does not "remember" the details of its formation).

The composite nucleus in a specific excited state can undergo various transformations, each with a ***certain probability*** of occurring (branching ratios). The composite nucleus remains in an excited state for a duration sufficient for a significant portion of its excitation energy to concentrate on a nucleon or a small group of nucleons, which will subsequently be ejected [21].

## 4. The direct interaction model

In the direct interaction model, it's assumed that the incident particle interacts with only one nucleon at a time, while the "core" of the nucleus remains inert or undergoes simple motion. The interaction time is on the order of the time required for the incident particle to traverse the target, and the angular distribution of the emerging particles is sharply peaked forward. This type of interaction is predominantly observed in reactions where a nucleon is ejected or stripped from the nucleus. The essential characteristics of direct interactions are observed at energies where the wavelength of the incident particle is smaller than the average spacing between nucleons in the target, encompassing magnitudes of several tens of *MeV* in the case of the incident neutron [41].

**IV. Radiative capture reaction (n, γ)**

**1. Definition**

Nuclei in highly excited states most commonly undergo de-excitation through the emission of a heavy particle, when it's energetically feasible. Below the dissociation energy, which refers to the binding energy of the last neutron, proton, or alpha particle, depending on which of these energies is the lowest, de-excitation can only occur through electromagnetic interaction. In this process, the nucleus transitions to a lower level or its ground state, analogously to excited atoms emitting light. However, the electromagnetic quanta emitted by the nucleus are predominantly on the order of $10^4$ to $10^6$ times more energetic than photons in the visible spectrum.

The gamma ray **γ** is, in fact, a monochromatic and highly penetrating form of electromagnetic radiation (consisting of high-energy photons). The relationship between the energy **E** and the wavelength **λ** of an electromagnetic quantum is as follows [42]:

$$\mathbf{E = h\nu} = \frac{hc}{\lambda} = \frac{1239{,}8}{\lambda} \qquad \textbf{(MeV)} \qquad\qquad \textbf{(1-12)}$$

Where:
**E** : energy (J or MeV)
**h** : Planck's constant (h = 6,62607015 × $10^{-34}$ J.Hz$^{-1}$ or J.s)
**ν** : frequency (Hz or s$^{-1}$)
**c** : speed of light (c = 299792458 m/s)
**λ** : wavelength is in fermi ($10^{-15}$ m)

**2. Mechanism of the radiative capture reaction (n, γ)**

Radiative capture occurs through the formation of a compound nucleus by the absorption of an incident neutron. The resulting nucleus possesses a high excitation energy, which is the sum of the kinetic energy of the incident neutron and its binding energy within the compound nucleus.

When the excitation energy of the nucleus exceeds the dissociation energy of a neutron or a proton, the nucleus undergoes decay through particle emission. However, below the dissociation energy, where de-excitation typically occurs through electromagnetic interaction, the nucleus undergoes de-excitation by emitting a photon.

$$_0^1 n + {}_Z^A X \rightarrow {}_Z^{A+1} X^* \rightarrow {}_Z^{A+1} X + \gamma$$
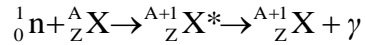
The return of the compound nucleus to its ground state can occur through the emission of a single highly energetic photon or gradually through intermediate levels of excitation, accompanied by the emission of multiple photons (referred to as a cascade).

The binding energy of the last neutron in most nuclei is approximately 7 to 8 MeV. This implies that after the capture of a slow neutron, the nucleus enters an excited state with an energy $E \approx 7$ to 8 MeV. From this state, it transitions back to the ground state, either directly or through one or more intermediate levels. The resulting gamma spectrum does not enable the precise determination of the positions of the levels.

The radiative capture reaction is employed in radiation protection due to the emission of potentially energetic photons. Generally, the cross-sections for radiative capture vary, with the exception of low energies where they exhibit a 1/V dependence, where V represents the velocity of the incident neutron [42].

### 3. Energetics of γ decay

Let's consider the decay of a nucleus with mass **M** at rest from an initial excited state **$E_i$** to a final state **$E_f$**. In order to conserve momentum, the final nucleus will not be at rest but must have a recoil momentum **$P_R$**, corresponding to a recoil kinetic energy **$T_R$**, assuming a non-relativistic scenario (**$T_R = P_R^2/2M$**).

The conservation of total energy and momentum gives :

$$E_i = E_f + E_\gamma + T_R \tag{1-13}$$

$$0 = \vec{P_R} + \vec{P_\gamma} \tag{1-14}$$

$$0 = P_R - P_\gamma \tag{1-15}$$

It follows that : $P_R = P_\gamma$ ;

(The recoil nucleus has a momentum equal and opposite to that of the γ radius).

$\Delta E = E_i - E_f$ and using the relativistic relation $E_\gamma = cP_\gamma$,

$$\Delta E = E_\gamma + \frac{E_\gamma{}^2}{2M\,c^2} \tag{1-16}$$

Who has the solution

$$E_\gamma = Mc^2 \left[ -1 \pm \left( 1 + 2\,\frac{\Delta E}{M\,c^2} \right)^{\frac{1}{2}} \right] \tag{1-17}$$

The energy differences $\Delta E$ are typically on the order of MeV, while the rest energy $Mc^2$ is on the order of $A \times 931.5$ MeV, where A represents the mass number [42].

$$E_\gamma \cong \Delta E - \frac{(\Delta E)^2}{2M\,c^2} \tag{1-18}$$

### 4. Average life and width of excited states

When the excitation energy of a nucleus exceeds the dissociation energy of a neutron or a proton, the nucleus undergoes decay through the emission of particles. This decay process is extremely rapid, with the corresponding average lifetime typically being less than $10^{-29}$ s. However, below the dissociation energy, where de-excitation normally occurs through

electromagnetic interaction, the average lifetimes are much longer, ranging from approximately $10^{-17}$ s to several years. The energy distribution of photons emitted by a source with an average lifetime $\tau$(s) resembles a resonance curve with a width (at half-maximum) given by:

$$\boldsymbol{\Gamma} = \frac{\hbar}{\tau} = \frac{6.58 \times 10^{-16}}{\tau} \qquad (\boldsymbol{eV}) \tag{1-19}$$

Where:

$\boldsymbol{\Gamma}$ : width (at half-maximum) (J or eV)

$\hbar$ : the reduced Planck's constant ($h/2\pi$) ($\hbar = 1{,}054571818 \times 10^{-34}$ J.s)

$\boldsymbol{\tau}$ : average life (s)

Consequently, the determination of the average life can be done by measuring either $\boldsymbol{\tau}$ or $\boldsymbol{\Gamma}$ [42].

### 4.1. Direct measurement of average life $\tau$

Reasonably long nuclear lifetimes can be directly measured by observing the decay of counting rates obtained from a source as a function of time. With fast electronic circuits, this method enables the measurement of average lifetimes up to approximately $10^{-5}$ s.

For much shorter average lifetimes, one of the most commonly used methods is the delayed coincidence technique. This method requires that the triggering pulse be electronically delayed, allowing the observation of coincidences between it and the de-excitation pulse. When an event is recorded by a gamma counter, the delay time represents the exact lifetime of the state or nucleus emitting the gamma radiation. The coincidence method enables the measurement of average lifetimes down to $10^{-11}$ s [42].

### 4.2. Measurement of natural width $\Gamma$

The extremely short average lifetime of $10^{-17}$ s corresponds to a "large" natural width of $\Gamma = 65{,}8$ eV. Only certain transitions that emit gamma rays with relatively high energies

(example : 6 MeV) exhibit such large natural widths. To directly observe natural widths, gamma spectrometers with high resolution capabilities are required.

One of the methods used to measure natural widths involves quantifying the probability, or cross-section, of gamma radiation absorption by a nucleus in its ground state.

When the incident gamma ray energies have a uniform distribution covering the entire width of the level to which the nucleus transitions, the absorption cross-section is proportional to this width. This method was employed by Booth for measuring the lifetimes of excited states ranging from $10^{-13}$ to $10^{-15}$ seconds (1964) [42].

## 5. Selection rules

Low-energy excited states decay through the emission of a gamma ray γ, thus the electromagnetic radiation can be described by a multipole expansion.

Electric multipole radiations, such as dipole, quadrupole, electric octupole, etc., are denoted as E1, E2, E3, and so on. Similarly, magnetic multipole radiations are referred as M1, M2, M3, and so forth.

The possible multipolarities for transitions between states **a** and **b** are given by [42]:

$$|\mathbf{J}_a - \mathbf{J_b}| \leq l \leq \mathbf{J}_a + \mathbf{J_b} \tag{1-20}$$

$\mathbf{J_a}$ and $\mathbf{J_b}$ are the angular moments of states **a** and **b**, $l$ is the multipolarity of radiation.

The photon has a spin 1 (*l must not be zero*), so there is no monopolar radiation.

The parity of the nucleus may or may not *change* during a multipolar transition.

The rule for the combination of parities of the initial and final states in an ***electric multipolar transition*** [42]:

$$\pi_a\pi_b=(-1)^l \tag{1-21}$$

For a ***magnetic multipolar transition*** :

$$\pi_a\pi_b=(-1)^{l+1} \tag{1-22}$$

So

$$\Delta\pi = \mathbf{no} : \quad \text{even electric, odd magnetic}$$

$$\Delta\pi = \mathbf{yes} : \quad \text{odd electric, even magnetic}$$

| Type | Symbol | Parity change |
|---|---|---|
| Electric dipole | $E1$ | Yes |
| Magnetic dipole | $M1$ | no |
| Electric quadrupole | $E2$ | no |
| Magnetic quadrupole | $M2$ | yes |
| Electric octupole | $E3$ | yes |
| Magnetic octupole | $M3$ | no |
| 16-pole electric | $E4$ | no |
| 16-pole magnetic | $M4$ | yes |

**Table 1.5.** Selection rules for gamma transitions [42].

*Table 1.5* summarizes the rules we have just provided regarding the variations of angular momentum and parity during a given multipolarity transition. These rules are referred to as selection rules for gamma transitions.

It should be noted that, in general, between two given states, a transition can occur with more than one multipolarity. For instance, if the initial and final states have angular momenta and

parities of $J_a = 1^+$ and $J_b = 2^-$, the possible values for the multipolarity, $l$ , are 1, 2, and 3. Since the parity changes, the possible transitions are E1, M2, and E3. In general, the transition probability decreases rapidly as the multipolarity $l$ increases. Therefore, in practice, we can often neglect all possible values of $l$ except the lowest one. In the above example, the transition will predominantly be an electric dipole radiation [42].

## 6. Internal conversion

A nucleus in an excited state can have a transition to a lower state either through gamma emission or internal conversion. In the latter process, the available energy and changes in angular momentum are transferred to an orbital electron, which is subsequently ejected [42].

**V. The Cross-Section**

In contrast to charged particles like electrons, which experience collisions with atoms in the medium along their trajectory and gradually slow down, photons and neutrons travel long distances between two collisions. However, in a single collision, they can lose a significant portion of their energy. To characterize the probability of an interaction occurring, the concept of cross-section (CS) is employed [43].

The cross-section of a nuclear reaction is related to the likelihood of its occurrence. Therefore, it serves as a characteristic quantity for its probabilities. There are two types of cross-sections: ***microscopic cross-section*** and ***macroscopic cross-section*** [34]

**1. Microscopic Cross-Section**

The microscopic cross-section represents the probability of encountering a single nucleus with an apparent surface area σ, as depicted in ***Figure 1.13*** [44].
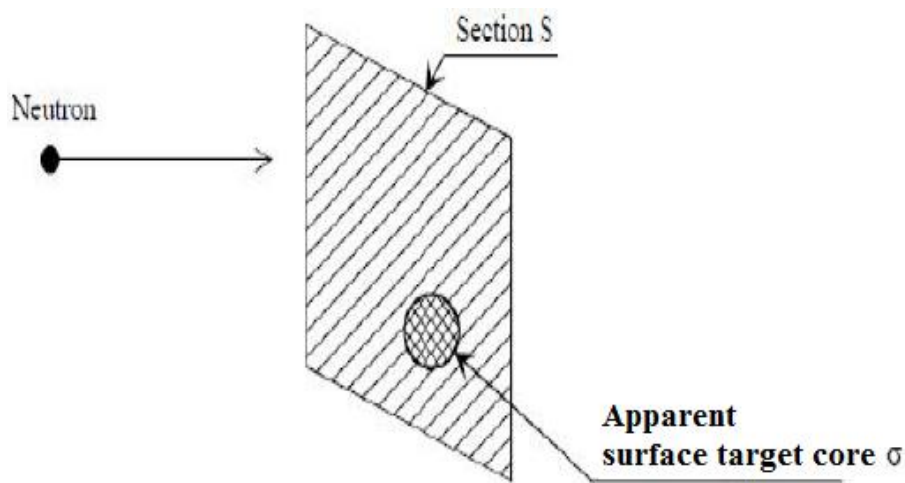


**Figure 1.13.** Schematic of neutron interaction with a target nucleus

of apparent surface area [44].

The microscopic cross-section depends on the nature of the target nucleus, the neutron velocity, and the resulting interaction. It's expressed in square centimeters, with the unit of measurement known as the barn, denoted as [44]:

$$1\ barn = 10^{-24}\ cm^2$$

The cross-section is given by:

$$\sigma = \frac{R}{n\,\Phi} \quad \rightarrow \quad R = n\,\Phi\,\sigma \qquad (1\text{-}23)$$

Where:

$\emptyset$ : The flux

**n** : The total number of target nuclei

$\sigma$: Cross-section

**R**: Reaction rate

The total cross-section is defined as:

$$\sigma_t = \sigma_s + \sigma_a \qquad (1\text{-}24)$$

The cross-sections for absorption $\sigma_a$ and scattering $\sigma_s$ are:

$$\sigma_a = \sigma_f + \sigma_c \qquad (1\text{-}25)$$

$$\sigma_s = \sigma_e + \sigma_{in} \qquad (1\text{-}26)$$

Where:

$\sigma_f$ : Fission Cross-Section

$\sigma_c$ : Capture Cross-Section

$\sigma_e$ : Elastic Scattering Cross-Section

$\sigma_{in}$ : Inelastic Scattering Cross-Section

## 2. Macroscopic Cross-Section

For a target of a certain thickness x, consisting of multiple atomic layers, the macroscopic cross-section is simply the microscopic cross-section multiplied by the density of target nuclei. If we consider a target containing multiple nuclei, the definition of the macroscopic cross-section remains the sum of the macroscopic cross-sections of the individual nuclei. It's given by [44]:

$$\sum = N \times \sigma \qquad \text{(1-27)}$$

Where :

$\sum$ : Macroscopic cross-section ($cm^{-1}$)

**N** : Atomic density (atoms/$cm^3$)

**σ** : Total cross-section (b or $cm^2$)

A cross-section can be "microscopic," meaning characteristic of an individual "target," or "macroscopic," meaning characteristic of a material containing a large number of targets [18].

## 3. Measurements of Neutron Cross-Sections

Among the fundamental data required for calculating the physical characteristics of nuclear reactors, cross-sections play an essential role. Over the past 70 years, these cross-sections have been measured using various techniques that are continually being developed to improve the accuracy and completeness of neutron cross-section data for stable and radioactive nuclei. Indeed, their energy dependence cannot be adequately described by a single predictive theory. To establish the necessary cross-sections for neutron calculations, procedures based on both experimentation and theory are required, along with associated uncertainties.

Cross-sections measurements in the energy range 10 keV to several MeV are frequently carried out with nuclear reactions induced by light ions which lead to monoenergetic or quasi-monoenergetic neutrons. Typically, a source reaction is chosen to produce neutrons of one energy (with low energy scattering), and these neutrons can be time continuous or pulsed. For the latter

type of source, TOF techniques can be used to reject parasitic neutrons of other energies. TOF is also commonly used in neutron scattering and emission measurements where the energy of the outgoing neutron is determined by the time of flight [45].

### *The neutron time-of-flight method (TOF)*

The most widely used experimental method to determine the cross section is that of the **time of flight** or **TOF**. There is a possibility to measure the energy of the neutrons, namely to measure its speed and also the time of flight between two points which is determined by the detector (most often a scintillator containing Li) which gives a very precise time signal when a neutron arrives. The second time signal is obtained for example by creating the neutrons by a reaction during which a charged particle appears at the same time, the recording of which is used as a starting signal.

The principle of neutron time-of-flight measurements is based on the pulsed neutron source which at an instant $t_0$ produces neutrons in a wide energy range. For reaction measurements, a sample is placed in the neutron beam at a well-known distance **L** and the reactions are observed with a detector. The detection of the reaction determines the time of arrival $t_n$ of the neutron on the sample and therefore its speed $v = L / (t_n - t_0)$, which gives the kinetic energy of the neutron. The idea is illustrated in the following *Figure 1.14* [45].
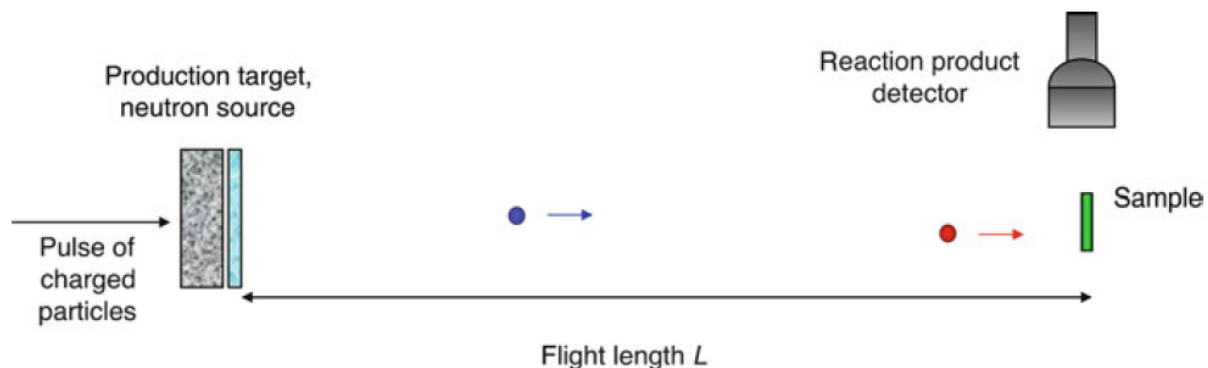


**Figure 1.14.** Principle of the neutron time-of-flight method [45].

Accelerator-based pulsed neutron sources are usually either electron-based sources where neutrons are produced via Bremsstrahlung on a high **Z** target, or proton-based sources where neutrons are produced by spallation on a heavy nucleus target.

The neutrons created by the pulsed source travel the flight path with a length **L** for a time **t** before possibly undergoing a reaction in a capture, diffusion or fission configuration, or before being detected in a transmission experiment. The kinetic energy of neutrons is determined relativistically from the velocity of the neutrons **v = L/t** and the momentum **p = mv** as;

$$E_n = E_{tot} - mc^2 = \sqrt{c^2 p^2 + m^2 c^4} - mc^2 = mc^2 (\gamma - 1) \tag{1-28}$$

with $\gamma = (1 - v^2 / c^2)^{-1/2}$ where **c** is the speed of light. For low energies where **v ≪ c**, which leads to the classical definition of kinetic energy

$$E_n \approx \frac{1}{2} m \, v^2 = \alpha^2 \frac{L^2}{t^2} \tag{1-29}$$

Taking the definition of the speed of light **c = 299 792 458 m/s** and taking **m = 939.6 MeV/c$^2$** for the neutron mass, we get **α = 72.3 μs $\sqrt{eV}$/m** using the units eV, m and μs for **E$_n$**, **L** and **t** respectively [45].

This is the rough method. The more refined method consists in constructing the response matrix of the detector and deconvolute the time of flight spectra to reconstruct the energy spectra. This because the measured TOF spectra is the time of flight plus the time spent in the moderator and detector (thus is a distribution of time). Even if we use monochromatic neutrons, the time spectra at the detector is always a distribution.

# Chapter 2

# Maxwellian Averaged Cross

# Section (MACS)

# *Chapter 2*

# *Maxwellian Averaged Cross Section (MACS)*

**I. Maxwellian Averaged Cross Sections (MACS)**

**1. Introduction**

Neutron-capture reactions play an important role in astrophysics and nuclear energy applications. The knowledge of the neutron capture cross sections of many isotopes are the fundamental ingredients for the calculation of stellar reaction rates used in astrophysical network calculations for obtaining the abundance distribution of the isotopes and elements in the universe.

The nucleosynthesis of the elements beyond iron is mainly produced by the so called s- and r-processes, which consist of successive neutron-capture reactions and subsequent beta decays. At the stellar sites, where s-process nucleosynthesis takes place, neutrons are quickly thermalized and exhibit a Maxwell–Boltzmann spectrum corresponding to the temperature T or energy kT typical of the mass and evolutionary stage of the star [46]. At kT= 30 keV the temperature at which, most of the stars spent their life, thus it's usually used as reference.

Cross sections are dependent on the energy of the particle in question. When dealing with a collection of particles at different energies, it is useful to get one number for the collection. This is done by averaging the cross sections over the energy distribution (Maxwellian) of the particles. The Maxwellian Averaged Cross Section (MACS) is the average cross-section measured for an given temperature T corresponding to an energy kT that is most probable on a spectrum of neutrons produced, represented by a Maxwell-Boltzmann distribution, and used for activation of samples [47].

## 2. Nucleosynthesis beyond Iron

The ashes of the big bang consist predominantly of nuclei of hydrogen and helium. The ashes themselves are subsequently burned in the nuclear fires of the stellar interiors with the metallic elements as residue.

The increasing densities and temperatures in stellar interiors provide the necessary environment in which all elements up to the region of the iron peak can be synthesized by charged-particle-induced nuclear reactions.

The sharp drop in the elemental abundances from A = 1 to A = 50 (*Figure 2.1*) reflects the fact that the Coulomb barrier, rising as the nuclear charge increases, increasingly impedes the reactions required to synthesize these elements. An exception to this general trend of the abundance curve is the iron peak (A ~ 56), because iron has the greatest stability of the nuclei involved in the rearrangement processes [47].
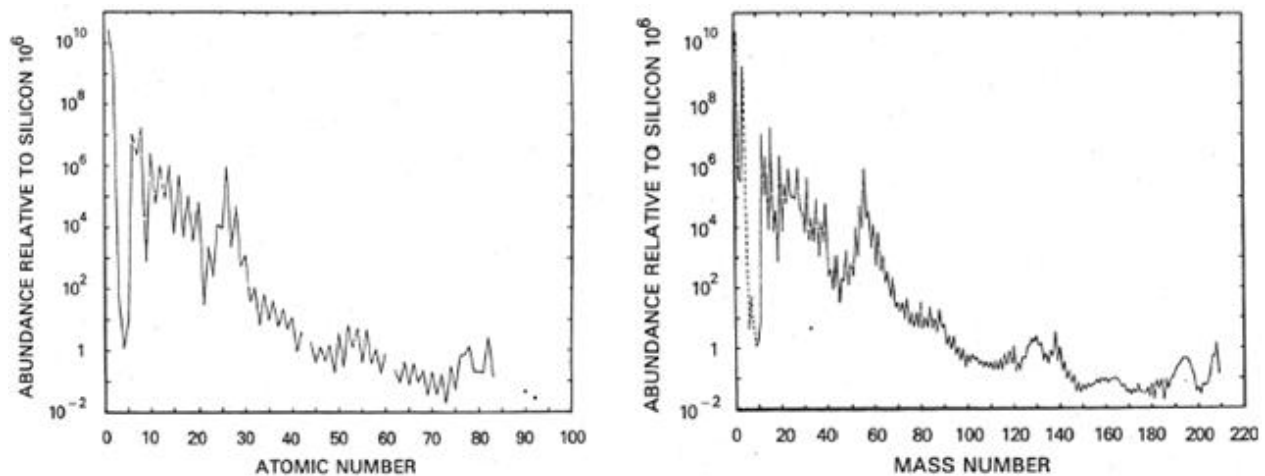


**Figure 2.1.** The abundances of both elemental and isotopic (nuclidic) species
in the solar system are presented [47].

The abundances are normalized in such a way that Si has the value $10^6$. Note the enormous abundance range displayed a factor of about $10^{12}$ from the most abundant element (H) to the least abundant elements shown.

If the heavier elements above the iron peak their abundances would drop very steeply with increasing mass, the observed abundance curve of the heavy elements exhibits a much slower decrease with mass number with double peaks labeled r and s in ***Figure 2.2***. Obviously these peaks are associated with neutron shell filling at the magic neutron numbers N = 50, 82, and 126.

The details of nucleosynthesis in stars by neutrons were involving neutron capture and β-decay for nucleosynthesis. The synthesis proceeds in steps at a slow rate (s-process) or at a rapid rate (r-process). That these two types of neutron-capture processes are required is dictated predominantly by the abundance data (***Figure 2.2***) [47].
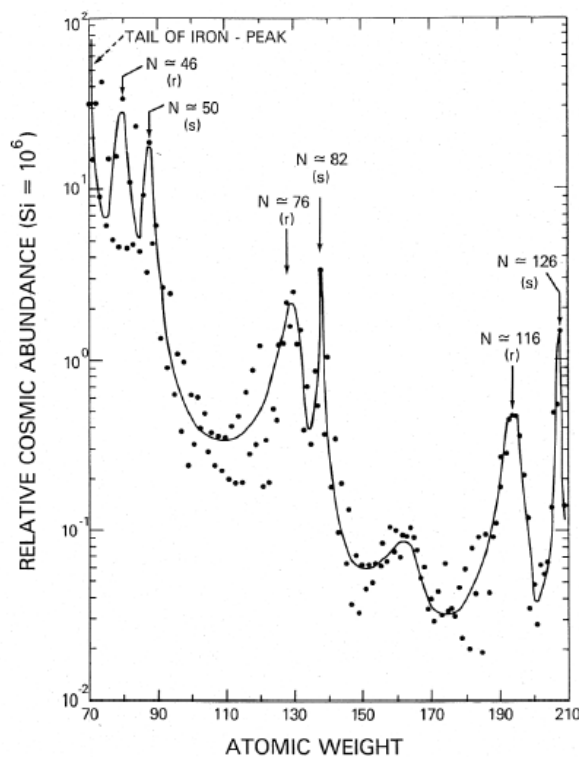


**Figure 2.2.** Cosmic abundances of heavy elements as a function
of atomic weight [47].

The line through the data points is to guide the eye. Note the narrow peaks for nuclei with closed neutron shells (N = 50, 82, and 126) and the broader peaks for nuclei mass units below the closed neutron shells.

The above hypothesis is supported by the following features [47]:

(1) The neutron-capture cross sections of the heavy elements are very large compared with those of the light elements (*Figure 2.3*), i.e., the heavy elements eagerly absorb neutrons.

(2) As pointed out above, the abundance curve (*Figure 2.2*) has structure, which can be explained only by neutron-capture reactions.

(3) The formation of heavy elements in stars by neutron capture occurs and is a continuing process.
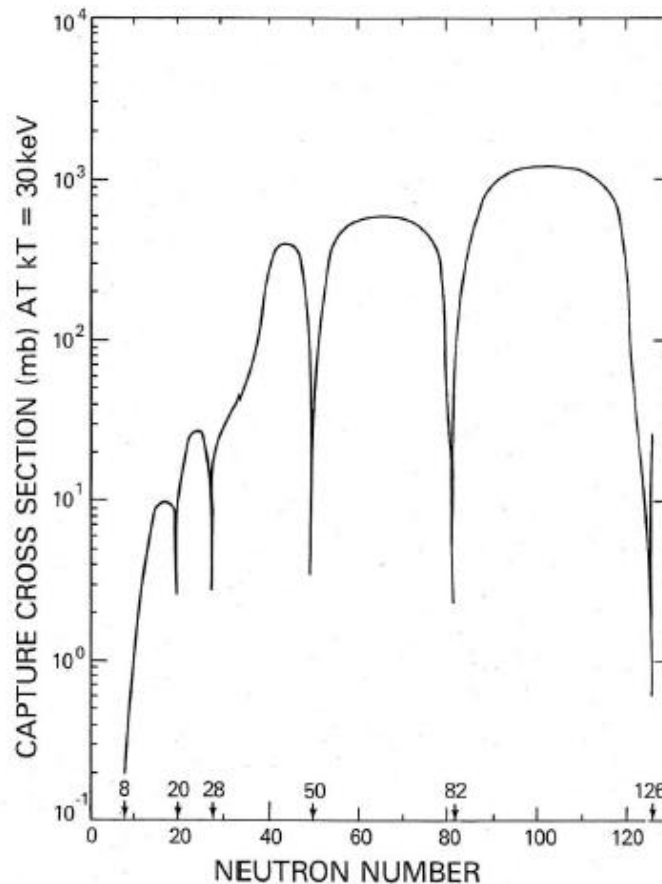


**Figure 2.3.** The measured average neutron-capture cross sections ($<\sigma>$) at 30 keV as a function of the neutron number (N) of the nuclei [47].

Note the large dips near the neutron closed shells at N = 8, 20, 28, 50, 82, and 126 [47].

## 3. Basic Mechanisms for Nucleosynthesis beyond Iron

As a result of each (n, γ) capture reaction, a nucleus (Z, A) is transformed into the heavier isotope (Z, A + 1). If this isotope is stable, an additional neutron capture leads to the isotope (Z, A + 2), and so on. Thus (n, γ) reactions increase the mass number by one unit at a time, providing the mechanism for synthesizing the elements beyond iron. If, in this Chain of capture reactions, the final isotope produced is unstable, subsequent processes depend on the intensity of the neutron flux impinging on the nuclei as well as on the lifetimes of the unstable nuclei against β-decay.

For unstable nuclei, when the time between successive neutron captures is much larger than the β-decay lifetimes, the network of processes involved is called the s-process ('slow'). Inspection of a chart of the nuclides reveals that the s-process closely follows the valley of β-stability. A section of the nuclear chart is shown in *Figure 2.4*.

If neutron capture proceeds on a rapid time scale compared with β-decay lifetimes, the network of reactions involved is called the r-process ('rapid' ) [47].
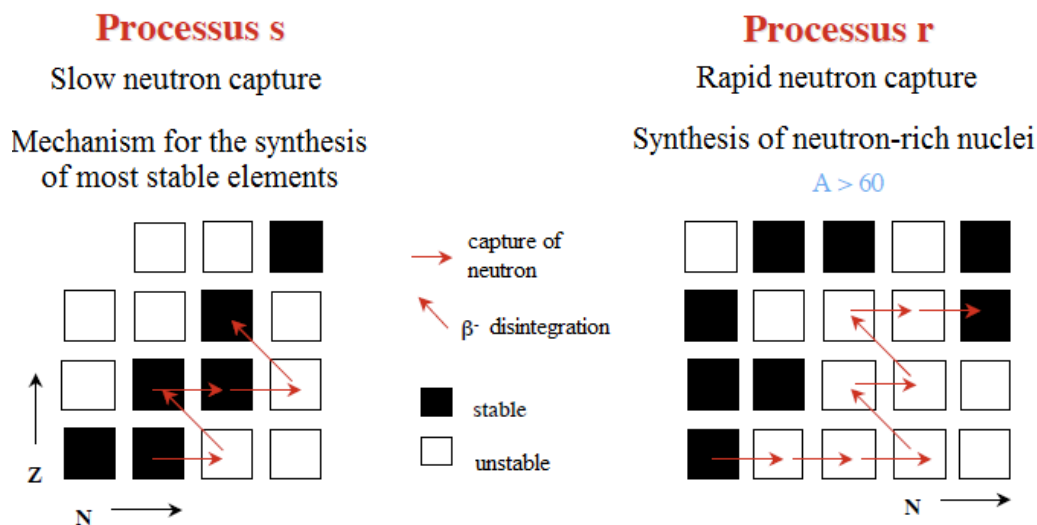


**Figure 2.4.** Neutron capture paths for s-process and the r-process [47].

## 4. Neutron-Capture Cross Section

The neutrons produced in stellar interiors are quickly thermalized through elastic scattering (in about $10^{-11}$ s), after which their velocities are represented by a Maxwell-Boltzmann distribution. Since the expected energy dependence of the neutron-capture cross section has the form:

$$\sigma_{n\gamma} \propto \frac{1}{v} \propto \frac{1}{E^{1/2}}$$

(2-1)

The most probable energy for the process to occur is near $E_0 = kT$ (*Figure 2.5*), or, equivalently, the most probable velocity is $V_T = (2kT / \mu)^{1/2}$, with $\mu$ as the reduced mass (for the neutron-target system) [47].
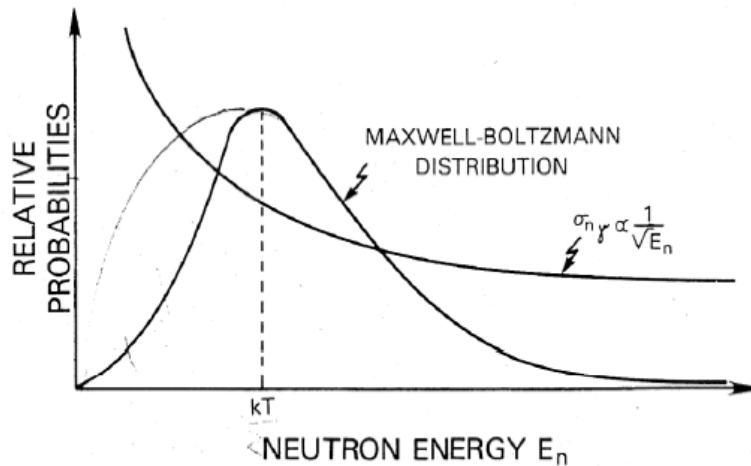


**Figure 2.5.** The Maxwell-Boltzmann energy distribution and the expected energy dependence of the neutron-capture cross section [47].

The stellar neutron capture rate [48]:

$$\langle \sigma v \rangle = \int_0^\infty \sigma v \phi(v) dv$$

(2-2)

45

Is determined by integration over the velocity distribution $\phi(v)dv$. Most neutron capture scenarios are associated with dense, he rich environments where neutrons are quickly thermalized, regardless of their production reactions. The resulting Maxwell–Boltzmann distributions [48]:

$$\phi(v)dv = \frac{4}{\sqrt{\pi}}\left(\frac{v}{v_T}\right)^2 exp\left(-\frac{v}{v_T}\right)^2 d\left(\frac{v}{v_T}\right)$$

(2-3)

Maxwellian-averaged stellar (n,γ) cross sections $\langle\sigma\rangle$ are defined as [48]:

$$\langle\sigma\rangle_{kT} = \frac{\langle\sigma v\rangle}{v_T} = \frac{2}{\sqrt{\pi}}\frac{\int_0^\infty \sigma(E_n)E_n\, exp(-E_n\,/\,kT)dE_n}{\int_0^\infty E_n\, exp(-E_n\,/\,kT)dE_n}$$

(2-4)

where $E_n = E_{n,lab}\,(A/(A + 1))$ is the total kinetic energy in the center-of-mass system, $E_{n,lab}$ is the laboratory neutron energy, $A$ is the number of nucleons of the target, $v_T = \sqrt{2kT/\mu}$ is the mean velocity, and $\mu$ is the reduced mass for the neutron-target system [48].

The Maxwellian-averaged cross sections $\langle\sigma\rangle$ is given then by [47]:

$$\langle\sigma\rangle = \frac{\langle\sigma v\rangle}{v_T} = \frac{2}{\sqrt{\pi}}\frac{1}{(kT)^2}\int_0^\infty \sigma(E)E\, exp\left(-\frac{E}{kT}\right)dE$$

(2-5)

($k$ Boltzmann constant $= 8,6173.10^{-5}$ eV.K$^{-1}$; $T$ = temperature, in K).

In the neutron energy range of interest for s-process nucleosynthesis ($E_n = 1$-300 keV), capture cross sections can be measured using several different techniques and a variety of neutron sources. Neutrons are produced most efficiently using accelerators. Electron linear accelerators (linac) and Van de Graaff accelerators (VDG) are most frequently used for this type of Work, each having specific advantages.

An electron linac, provides a very powerful neutron source. Intense neutron bursts with broad energy distributions are produced by pulsed high-power electron beams via ($\gamma$, n) reactions on heavy-métal targets. With this time structure, capture cross section measurements can be carried out with excellent neutron energy resolution using time-of-flight (TOF) techniques in combination with flight paths of about 50 m. A problem with the linac is the intense bremsstrahlung from the neutron target, which requires heavy shielding of the target area.

In contrast to a linac, the VDG accelerator produces neutron fluxes smaller by 3-4 orders of magnitude. However, because the ion beams used for neutron production do not generate bremsstrahlung radiation, the need for target shielding is greatly reduced. As a consequence, significantly shorter neutron flight paths (<60 cm) can be used. This, in turn, allows the use of larger solid angles that compensate to a large extent for the lower neutron source strength. The (p, n) reactions on $^7$Li or $^3$H are used most commonly for neutron production. The proton energy is adjusted slightly above the reaction threshold, so that the center-of-mass velocity of the system exceeds the velocity of the emitted neutrons. In this situation the neutrons are kinematically collimated in a forward cone.

In most experiments, capture reactions are detected via the prompt y-cascades by which the newly formed nucleus de-excites. These so-called direct detection methods, which are supplemented by the activation technique.

Neutron capture leads to an unstable nucléus, measurements of the activity of these nuclei can be used to determine the capture rate. In this case the sample is placed close to the neutron target (***Figure 2.6***) and irradiated over a specific time interval (adjusted to the half-life of the unstable nucléus produced) [47].
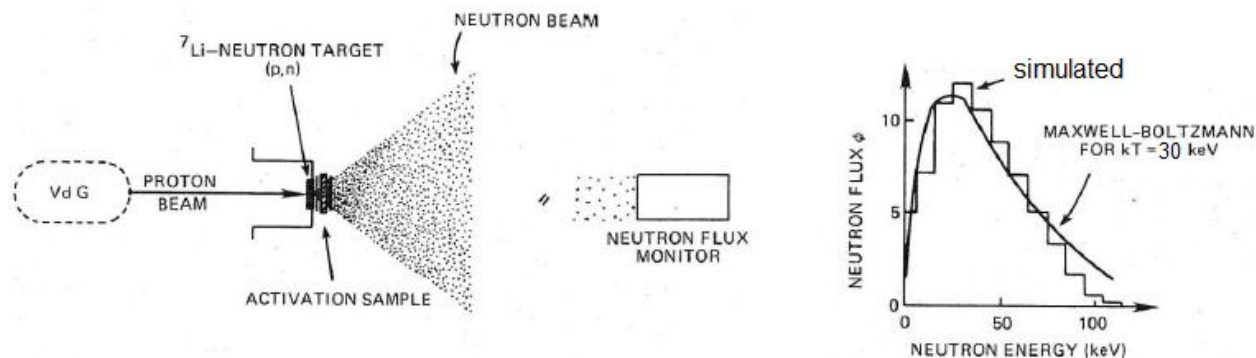
**Figure 2.6.** Schematic Setup for irradiating samples utilizing a kinematically collimated neutron beam [47].

All neutrons are emitted in a forward cone because of the reaction kinematics (for protons above threshold). The time dependence of the neutron flux and of its energy at zero degrees is monitored with a $^6$Li glass detector. The figure on the right shows the approximation to the Maxwell-Boltzmann energy distribution at kT = 30 keV (solid line) of the neutron spectrum simulated via the $^7$Li (p, n) $^7$Be reaction during activation (histogram).

The neutron source is shut off and the induced activity counted with calibrated high-resolution detectors. Measurement of the activity as a function of time is used to verify that the correct assignment was made of the (n, γ) reaction being studied. The basic advantage of activation measurements is their inherent sensitivity.

Since the activation technique provides an average cross section over the spectrum of the neutrons used for activation (***Figure 2.6***), the neutron spectrum must be accurately known. Many investigators have tried to circumvent this difficulty by using monoenergetic neutrons. Problem solved by tailoring a spectrum that almost perfectly matches the Maxwell spectrum for kT = 30 keV. This was possible because of the experimentally determined properties of the $^7$Li (p, n) $^7$Be reaction when using protons above threshold. The spectrum simulated with MCNPX is as shown in the histogram in the right part of ***Figure 2.6*** in 95% agreement with the Maxwell distribution for kT = 30 keV (solid line).

Thus activation measurements done with such a neutron spectrum already provide the proper Maxwellian average for the cross section [47]:

$$\langle\sigma\rangle = \frac{\langle\sigma v\rangle}{v_T} = \frac{2}{\sqrt{\pi}} \frac{\int_0^\infty \sigma(E)E \, exp\left(-\frac{E}{kT}\right)dE}{\int_0^\infty E \, exp\left(-\frac{E}{kT}\right)dE} \approx \frac{2}{\sqrt{\pi}} \overline{\sigma}_{exp}$$

(2-6)

The sample to be investigated is sandwiched between two gold foils (*Figure 2.6*). Since the neutron-capture cross section for gold is accurately known and it can be activated as well, gold serves as an in situ standard.

The experimental efforts of many research groups contributed data on the average capture cross section <σ> at 30 keV for a wide range of nuclei. These data are shown schematically in *Figure 2.3* as a function of neutron number N. Note that the light nuclei have small capture cross sections compared with the heavier ones (N > 28, A > 60). This feature is due in part to the low energy-level density in light nuclei, where often just a few resonances contribute to the capture cross section.

Note also the large dips that appear near the neutron closed shells with N = 8, 20, 28, 50, 82, and 126. These dips are caused by the dramatically reduced level density of nuclei with closed neutron shells as compared with neighboring nuclei. The data verify that the heavier elements are particularly likely to absorb neutrons [47].

## II. Generation of the neutron spectrum through the $^7$Li (p, n) $^7$Be reaction

### 1. Introduction

Measurements of the cross section as a function of neutron energy can be performed by measuring the activity (induced radioactivity) of the sample of interest after irradiation within the neutron spectrum, for transmission experiments using **$^6$Li** glass detectors ($^6$Li-glass), for (n, xnγ) measurements with HPGe detectors [45].

In the neutron energy range of interest for nucleosynthesis process ($E_n$ = 1-600 keV), capture cross sections can be measured using a variety of different techniques and a variety of neutron sources. Neutrons are produced most efficiently using accelerators [47].

In an accelerator (VDG), (p, n) reactions on $^7$Li are used for the production of neutrons whose spectrum must be known with precision [49] to determine reference energy at kT = 30 keV, which is in direct relation to the temperature (corresponds to a temperature of $3.5 \times 10^8$ K). This reference energy is represented by a Maxwell-Boltzmann distribution, and used for activation of samples [47].

The production of the neutron spectrum produced by MCNPX simulation of the neutron source obtained by the $^7$Li (p, n) $^7$Be reaction in an accelerator (VDG) which offers the possibility of adapting the neutron spectrum exactly to the range of stellar energy, most be adjusted with respect to a true Maxwell-Boltzmann distribution for energy of kT = 30 keV to have a good agreement [47].

### 2. Neutron energy distributions

The reaction $^7$Li(p,n)$^7$Be, at proton energies near above the reaction threshold can produce a good approximation to a MSNS (Maxwellian-Shaped Neutron Spectrum) [1], by providing large quantities of neutrons with energy ranging from a few up to hundreds keV [50].

When a monochromatic beam of charged particles interact with a thin foil of material, the outgoing beam energy is no more monochromatic because of electromagnetic interaction of the protons with the atoms of the material. Such a behavior can be used to change or "shape" the monochromatic proton energy distribution coming out from the accelerator [51].

The neutron spectrum production is based on the use of the $^7$Li(p,n)$^7$Be reaction [1] because it is one of the most prolific neutron-producing reaction in the keV neutron energy range [49], but using a shaped proton beam. The proton beam with 3.65 MeV, originating from the accelerator, is shaped through a thin foil of material (Aluminum (or Lead) : 70-125 μm), the energy of the monochromatic proton beam coming from the accelerator is shaped into a Gaussian like or convolution of Gaussian like distribution [1].

It should be stressed that the biggest advantage of the present approach is that no moderation system is used [1]  (a large amount of neutrons is often lost at the sample position, due to capture in the moderator) [50], while a high neutron flux is provided because of the use of a higher proton energy, even if large part of the proton beam is not used for the neutron production because its energy falls down to the threshold [1] of the $^7$Li (p, n) $^7$Be reaction of 1.88 MeV [50].

The $^7$Li(p,n)$^7$Be reaction yields a continuous energy distribution in a forward cone of 120$^°$ opening angle [52].
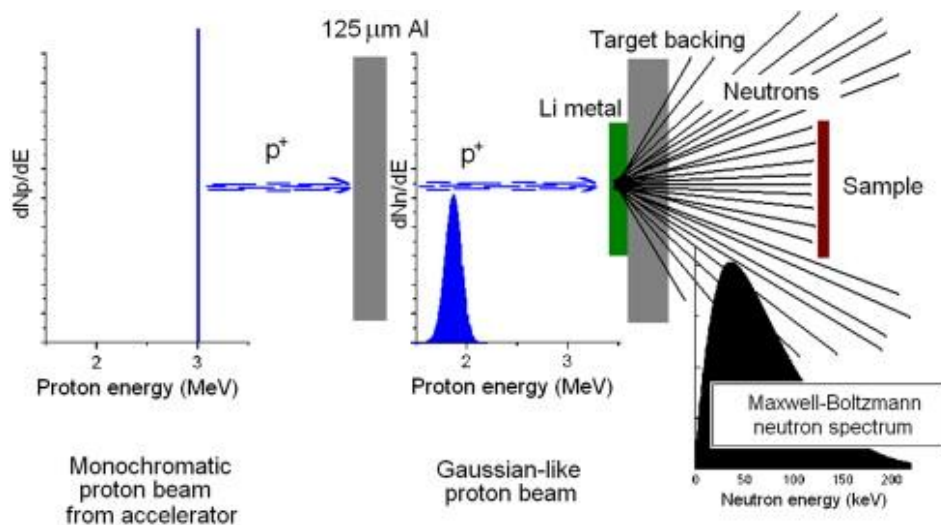


**Figure 2.7.** Setup for the beam line at CN

(7 MV Van Der Graaf accelerator at INFN-LNL) [49].

The shaped beam impinges on a thick metallic Lithium target producing a neutron field that activates a circular-shaped sample placed in front of it at a definite target-to-sample distance [49], the copper backing held the aluminum foil, the lithium layer and the sample [53].

The Gaussian proton distribution energy spectrum behind the aluminum foil is calculated with SRIM code (simulating the transport of protons through the energy shaper materials) [46, 50].

A computer code (LZYield code [54]): based on Thick target neutron yields for the $^7$Li(p,n)$^7$Be reaction near threshold [46]) was developed to study the behavior of the $^7$Li (p, n) $^7$Be reaction and its neutron yield for different proton energy distributions. With this code the desired Maxwell-Boltzmann neutron spectra is calculated tuning the shaped proton energy [1].

The effects of the target structure, mass and surrounding environment on the neutron spectra (take into account the full geometry of the target and neutron scattering in materials surrounding the target for the transport of neutrons with angular and energy yield of LZYield) can be simulated using MCNPX (Right the *Figure 2.6*) [1, 50], The inputs files are generated from the LZYield code for the source card in the MCNPX [50].

The free parameters used to produce the desired MSNS (Maxwellian-Shaped Neutron Spectrum) at given kT (30 keV) are the proton energy of the accelerator, the foil thickness (Al (or Pb)) and the angular aperture seen by the measuring sample [1]. For every set of these parameters a neutron spectrum is calculated and fitted to a Maxwell–Boltzmann function, determining the energy kT = 30 keV and the goodness of fit (coefficient of determination) for that fit [49].
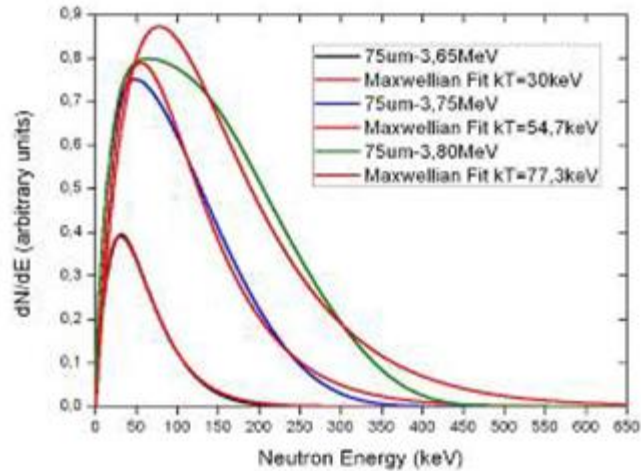
**Figure 2.8.** Maxwell Boltzmann neutron spectra (MBNS) at different stellar temperatures for different proton energies and 75 μm Al thickness [55].
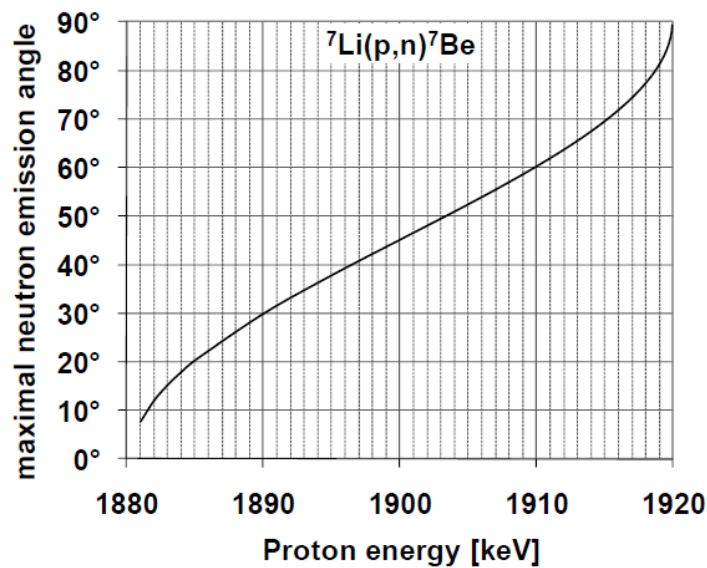


**Figure 2.9.** Near-threshold thick target neutron angular distributions for natural lithium metal [55].

In order to reduce the mass of the sample, when measuring rare elements of radioactive isotopes, a high intensity neutron flux is required [1]. Thus, it is of great importance to have the smallest possible proton beam spot size at the target and the sample as close as possible to it. This can be achieved maximizing the beam current and minimizing the beam cross area [50]. The

crucial element for neutron production within this approach is the Lithium target (some μm thick metallic Li target) [1].

Metallic lithium necessitates cautious handling due to its inherent chemical instability and potent oxidation potential. At ambient temperature, lithium readily reacts with both nitrogen and oxygen, forming a surface layer that diminishes the overall neutron yield. Consequently, the lithium foil has conventionally been stored in an environment saturated with inert gas or in vacuum to prevent its degradation [55].

The Lithium target assembly must satisfy to several constraints [55]:

1- Low mass: This is necessary to minimize neutron backscattering and to reduce radioactivity. The use of a low-mass Lithium target helps to mitigate these effects.

2- Small thickness: The target assembly should have a small thickness to maximize the neutron flux. By keeping the measuring sample in close contact with the neutron-producing surface, the neutron flux can be optimized. Additionally, a small copper backing thickness helps to minimize perturbations in the neutron spectra.

3- Low cost and easy fabrication procedure: The target material should be affordable and readily available, and the fabrication process should be straightforward. This enables the target to be replaced frequently, even during measurements, ensuring continuous and reliable experimental conditions.

The Aluminum (or Lead) shape foil material used must satisfy certain requirements [55]:

1- Low atomic number and low density: These properties are desirable to minimize neutron scattering and absorption, ensuring efficient transmission of neutrons through the foil material and, mostly, managing well the thickness disomhogenity.

2- High melting point: A high melting point is important to maintain the structural integrity of the foil material under the high-energy proton beam used for neutron production.

3- High thermal conductivity: Good thermal conductivity helps dissipate heat generated during the interaction between the proton beam and the foil material, ensuring stable operation and minimizing temperature fluctuations.

4- High tensile strength: The foil material should possess high tensile strength to withstand mechanical stresses and prevent deformation or breakage during handling and usage.

With such neutron spectra, using the activation technique it is possible to measure the MACS at 30 keV by measuring the total neutron capture cross section [1]. Upon subjecting the specimen to irradiation, in the event that the nucleus generated through the process of neutron capture exhibits radioactivity, characterized by a suitable half-life, the subsequent measurement of gamma activity enables the acquisition of the empirical neutron capture cross section [57]. The energy of 30 keV commonly used as a reference [56].

The value of the MACS at kT = 30 keV can also be obtained by correction (extrapolation or interpolation) to the measured value at kT = 25 keV (or another value), if a good approximation of the MSNS (Maxwellian-Shaped Neutron Spectrum) which depends on a given structure is at kT = 25 keV (or another good value) [1].

**III. Measuring of the Maxwellian Averaged Cross Section (MACS) at kT= 30 keV by Activation**

**1. Introduction**

By activation, the accuracy is much higher and the sample can have much less mass (convenient when you have radioactive isotopes samples, they are bad or not measured at all because of the large background). Moreover, the flux is much higher, allowing the measurement of low cross section (magic nuclei) or rare or costly elements. Furthermore, the activation technique cannot be applied if a stable or a short-lived isotope is produced in the neutron capture reaction.

Neutron activation analysis is an important method to quantify the activation foils. The activation foil becomes radioactive when it is irradiated by neutrons. The activated nuclides undergo decay and emit various kinds of particles. In most cases gammas are emitted with specific energies.

For each element studied, the capture reactions are detected via the y-cascades of new nuclei formed and excited in the irradiated sample.

The nuclear reaction cross section of the sample can be estimated by measuring the gamma activity of the nuclide using high resolution HPGe detector.

The measurement of the activity of these new nuclei is used to go back to the measurement of the Maxwellian Averaged Cross Section of the irradiated elements for a reference temperature T corresponding to an energy E = kT = 30 keV.

The Measure of the cross section for an element is relative to the cross section of $^{197}$Au, since the $^{197}$Au may also be enabled to serve as a standard. They use gold because of the high cross section, reasonable lifetime (which means a good statistic can be performed in a short time) and because the cross section is well known [52, 53, 55-60].

## 2. Measuring of the MACS for $^{197}$Au(n, γ) at kT= 30 keV by Activation

The setup consisted of a copper backing that held the metallic lithium target and the gold sample *Figure 2.10*. After the irradiation, $^{7}$Be is prodused (in the Lithium target) and $^{198}$Au (with a half-life of 53,29 and 2,6947 days respectively) [57, 59].
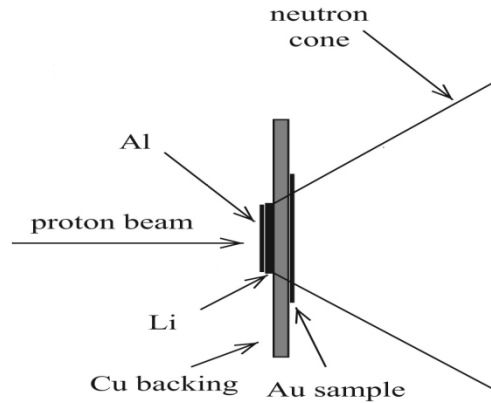


**Figure 2.10.** Experimental setup during the activations [55].

The cross section can be calculated if the number of activated nuclei **A**, the neutron fluence through the sample **Φ**, and the sample mass thickness **N** are known [57-59]:

$$\sigma_{exp} = \frac{1}{N_{Au}} \frac{A_{Au}}{\phi} = \frac{1}{N_{Au}} \frac{C_{Au}}{C_{Be}} \frac{[f_d.I_\gamma.\epsilon.K_\gamma]_{Be}}{[f_d.I_\gamma.\epsilon.K_\gamma]_{Au}} \frac{1}{K_s} \frac{1}{K_f}$$

(2-7)

*A*, the number of activated nuclei, can be determined from the γ-ray spectra measured with the HPGe detector. *C* is the number of events registered by the detector, *Iγ* is the gamma intensity of lines; *ε* is the HPGe gamma detector efficiency (including energy efficiency and geometric efficiency that takes into account the extended samples effects); *$K_\gamma$* is the correction due to the gamma absorption and scattering in materials, before the gammas reach the detector; *$K_s$* reflects the neutron scattering (meanly due to Cu backing but also due to the sample); *$K_f$* is a correction due to the flat sample used in experiment: it must be noticed that the Au sample thickness as seeing by neutrons passing through Au depends on the entering angle θ inside the sample *Figure 2.11*.
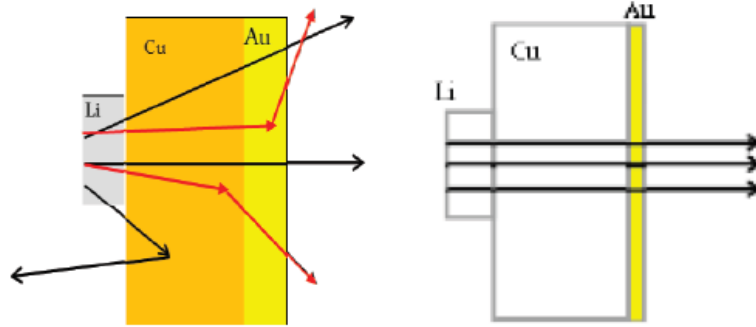
**Figure 2.11.** Left: scheme of some possible neutron scattering effects in a real experiment. Right: ideal activation experiment [59].

The factor $f_d$ relates the number of the decay nuclei during the measurement time ($t_m$) with the total number of activated nucleus (during irradiation time, $t_a$). It also includes the decay nuclei during the waiting time ($t_w$), the time between the end of neutron irradiation and the beginning of activity measurement with the HPGe detector, and $\Phi(t)$ is the neutron flux.

$$f_d = \frac{e^{-\lambda t_a}(\int_0^{t_a} \Phi(\tau)e^{\lambda \tau}d\tau)}{\int_0^{t_a} \Phi(\tau)d\tau}\left(e^{-\lambda t_w}\right)\left(1 - e^{-\lambda t_m}\right)$$

(2-8)

$C_{Au}$ and $C_{Be}$ are counted using Canberra GENIE2000 software connected to the acquisition system consisting of HPGe.

Mass thickness $N_{Au}$ is obtained with accurate measurements of mass and surface of the gold sample, cutting the gold sample after irradiation for a more precise measurement of the activated region.

Finally, in order to obtain the MACS, a correction is needed of experimental cross-section ($\sigma_{exp}$) due to the difference between a quasi-maxwellian neutron spectrum and a true maxwellian neutron spectrum at kT = 30 keV, so-called $K_{max}$ factor [57-59].

$$MACS = \frac{2}{\sqrt{\pi}}\, K_{max}\, \sigma_{exp}$$

(2-9)

### 3. Measuring of the MACS for elements at kT= 30 keV by Activation

The samples are typically sandwiched between gold foils and placed directly on the backing of the lithium target. A typical setup is sketched in ***Figure 2.12***. The simultaneous activation of the gold foils provides a convenient tool for measuring the neutron flux, since both the Maxwellian averaged neutron capture cross section of $^{197}$Au and the parameters of the $^{198}$Au decay are accurately known (The half-life of $^{198}$Au is 2.6947 days) [52].
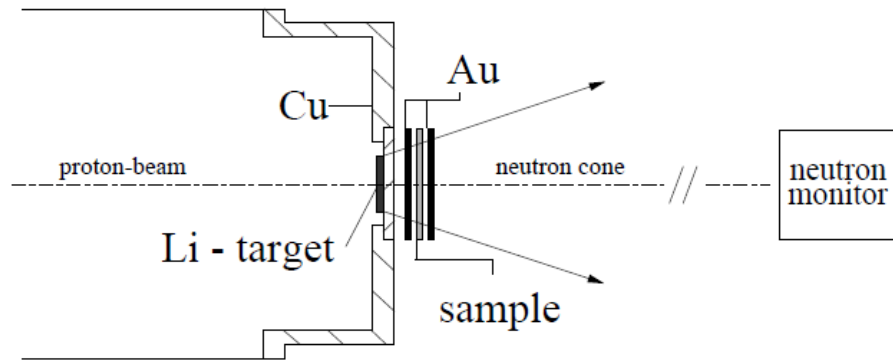


**Figure 2.12.** Typical activation setup (The sample is usually sandwiched by two gold foils in order to determine the neutron flux just before and behind the sample) [52].

The MACS of sample with gold as a reference can be obtained with the expression [53, 56]:

$$\textbf{MACS}_{\textbf{sample}} = \textbf{MACS}_{\textbf{Au}} \; \frac{n_{Au}\, f_{A-Au}\, \Phi_{Au}\, A_{sample}}{n_{sample}\, f_{A-sample}\, \Phi_{sample}\, A_{Au}} \tag{2-10}$$

where $\textbf{MACS}_{\textbf{Au}}$ is the MACS Au reference, $\textbf{\textit{n}}$ is the sample thickness (at/b), $\Phi$ is the fluence through the sample (determined by measuring the $^{7}$Be activity), $\textbf{\textit{A}}$ is the number of activated nuclei, $\textbf{\textit{f}}_{A-X}$ accounts the decay during the time of activation, $t_A$, of the isotope $\textbf{\textit{X}}$:

$$\textbf{\textit{f}}_{A} = \frac{\int_0^{t_A} \Phi(t) e^{\lambda(t-t_A)} dt}{\int_0^{t_A} \Phi(t) dt} \tag{2-11}$$

$\Phi(t)$ is the neutron flux as a function of the time. $A$ can be determined from the γ-ray spectra with the relation :

$$A = \frac{C}{K_\gamma \epsilon I_\gamma (1 - e^{-\lambda t_m}) e^{-\lambda t_w}}$$

<div align="right">(2-12)</div>

$C$ is the number of events registered by the HPGe detector, $K_\gamma$ is a correction factor for self-absorption and multiple scattering, $\epsilon$ is the detector efficiency, $I_\gamma$ is the absolute intensity for the particular gamma-ray line used for the measurement of the $^{198}$Au activity; $\lambda$ is the decay constant of each isotope and $t_m$ and $t_w$ the measuring and cooling times. In case of constant flux, Eq. (**2-8**) reduces to **(1-exp(-$\lambda t_A$))/$\lambda t_A$**.

The discrepancy in neutron fluence between the gold and sample materials arises from the placement of the sample behind the gold sample. These variations investigate through the utilization of MCPNX simulations, which facilitate the examination of the neutrons traversal through the gold front surface, the sample's front surface, and its back surface. By approximating the average reduction in sample flux, an estimation of the fluence ratio between the gold and sample can be derived [53, 56].

# Chapter 3

# Systematics of Maxwellian

# Averaged Neutron Capture

# Cross Sections (MACS) at

# 30 keV

# Chapter 3

# Systematics of Maxwellian Averaged Neutron Capture Cross Sections (MACS) at 30 keV

## 1. Introduction

A formula for the calculation of neutron radiative capture cross sections in the framework of a statistical model approach was proposed in the work of Y. Djerboua et al. [61]. In that work, a significant interrelation with experimental data shows that systematics is useful in estimating the (n,γ) cross sections of neighboring odd-A isotopes and even-even isotopes [62], where no experimental data are available. For unstable nuclei, experimental measurements of (n,γ) reaction cross sections are rather difficult due to the radioactivity of target material [63-66], and the difficulty of having enough nuclei to perform an experiment. From a theoretical point of view, it remains a challenge to estimate model parameters in a reliable way for calculating the (n,γ) reaction cross sections of nuclei far from the β-stability line [67-69]. Using the experimental data of nuclei available in the Karlsruhe Astrophysical Database of Nucleosynthesis in Stars (KADoNiS) [70], a MACS formula is derived for target nuclei with mass number A ≫ 1 and 30 keV incident neutron energies.

## 2. Theoretical background

### 2.1. Radiative cross section

From Bohr's postulate, for neutrons with energies below the pre-equilibrium region (around 14 MeV), the nuclear reaction process can be divided in two well-separated independent stages. The first is the formation of a compound nucleus in a well-defined state, in which the incident energy is shared among all the constituent nucleons. Then, the compound nucleus loses its memory of the formation process and goes to the second stage: decay happens through particle

emission (neutron, γ ray, proton…) or the fission process. The radiative (n,γ) cross section is the product of the formation cross section of the compound nucleus and the probability of its decay through γ emission, which is [61, 62]:

$$\sigma(\mathbf{n}, \boldsymbol{\gamma}) = \sigma_{cn} \frac{\Gamma_\gamma}{\Gamma} = \sigma_{cn} \frac{\Gamma_\gamma}{\sum_i \Gamma_i} \tag{3-1}$$

where $\sigma_{cn}$ is the formation cross section of the compound nucleus, $\Gamma_\gamma$ is the γ-emission width of the compound nucleus and, $\Gamma$ represents the total decay width which is the summation over all possible decay channels $\Gamma_i$. The (n,γ) cross section can be written as [61, 62]:

$$\sigma(\mathbf{n}, \boldsymbol{\gamma}) = \frac{\sigma_0 \Gamma_R^2 \rho(E^*)}{g m_n c^2 E_{GDR}^4 E_n} \left( 24 t^5 + \frac{1375.2}{E_{GDR}^2} t^7 \right) \tag{3-2}$$

where $c$ is the speed of light, $m_n$ is the neutron mass at rest, $E_n$ is the incident neutron energy, $\rho$ is the nuclear level density and, $E^*$ is the excited energy of the compound nucleus. The values of the empirical parameters of the giant dipole resonance (GDR) are: $\sigma_0 = 2.5\,A$ (mb), $E_{GDR} = 40.3\,A^{-1/5}$ (MeV), $\Gamma_R = 0.3\,E_{GDR}$ where, $t$ is the nuclear temperature and $A$ is the mass number of the compound nucleus. The spin statical factor ($g$) is given by [61, 62]:

$$g = \frac{(2s_n+1)(2s_d+1)}{(2s_c+1)} \tag{3-3}$$

where $s_n$, $s_d$ and $s_c$ are the spins of neutron, residual and compound nuclei, respectively.

Within the constant temperature (CT) model, the level density can be written as [61, 62]:

$$\rho(E^*) = \frac{1}{t} e^{(E^*-E_0)/t} \tag{3-4}$$

where $E_0$ is backshift energy.

### 2.2- Systematics for (n,γ) reaction cross sections of nuclei

The (n,γ) cross section is proportional to the level density of a compound nucleus with excitation energy $E^*$ (Eq. 3-2). The excitation energy is given by the mass-energy relation [61, 62]:

$$E^* = S_n(Z, A+1) + \frac{A}{A+1}\, E_n = [m(Z, A) + m_n - m(Z, A+1)]c^2 + \frac{A}{A+1}\, E_n \qquad (3\text{-}5)$$

where $S_n(Z,A+1)$ is the neutron separation energy of the compound nucleus.

For a ***non-magic*** target nucleus with $A \gg 1$, the value of $E^*$ can be calculated using the Weizsacker mass formula and reduced to [61, 62]:

$$E^* \approx c_1 - \frac{a_a}{4}\left[\frac{2(N-Z)+1}{A} - \frac{(N+1-Z)^2}{A^2}\right] + \frac{A}{A+1}\, E_n \qquad (3\text{-}6)$$

where $c_1$ is a constant along one isotopic chain and, $a_a = 92.80\ \text{MeV}$ is the parameter of the asymmetry terms in the formula. At the same incident energy $E_n$, approximately taking $\frac{A}{(A+1)} \sim 1$ [61, 62],

$$E^* \approx c_1 - \frac{a_a}{4}\left[\frac{2(N-Z)+1}{A} - \frac{(N+1-Z)^2}{A^2}\right] + E_n \qquad (3\text{-}7)$$

Combining Eqs. (3-2), (3-4) and (3-7), the isotopic dependence of (n,γ) cross section is written as [61, 62]:

$$\sigma(n, \gamma) = a\, A^{1.4}\, e^{-b\left[\frac{2(N-Z)+1}{A} - \frac{(N+1-Z)^2}{A^2}\right]} \qquad (3\text{-}8)$$

With,

$$a = \frac{1.385 \times 10^{-4}}{g m_n c^2 E_n} \left( 24 t^4 + \frac{1375.2}{E_{GDR}^2} t^6 \right) e^{(c_1 + E_n - E_0)/t} \quad \text{(mb)} \tag{3-9}$$

$$b = \frac{a_a}{4t} \tag{3-10}$$

where **a** (in millibarn units) and **b** are the adjustment parameters and; **A**, **N** and **Z** are the mass number, number of neutrons and number of protons of the target nucleus, respectively, with **A = N + Z** [61, 62].

## 3. Systematics for MACS at 30 keV

The neutron radiative capture cross section in the framework of a statistical model approach is calculated with Eq. (3-1). From this equation a formula for measuring the MACS at 30 keV is derived. The **MACS** is defined as the ratio between the reaction rate per particle rate ($\langle \sigma v \rangle$) and the most probable velocity ($v_T$) [47, 49, 71]:

$$\text{MACS} \equiv \langle \sigma \rangle_{kT} = \frac{\langle \sigma v \rangle}{v_T} = \frac{2}{\sqrt{\pi}} \frac{\int_0^\infty \sigma(E_n) E_n \, e^{\left( \frac{-E_n}{kT} \right)} dE_n}{\int_0^\infty E_n \, e^{\left( \frac{-E_n}{kT} \right)} dE_n} \tag{3-11}$$

$$\text{MACS} = \frac{2}{\sqrt{\pi}} \frac{1}{(kT)^2} \int_0^\infty \sigma(E_n) E_n \, e^{\left( \frac{-E_n}{kT} \right)} dE_n \tag{3-12}$$

where **T** is the stellar temperature, **k** is the Boltzmann constant, $E_n$ is the incident neutron energy and $\sigma(E_n)$ is the energy dependent neutron capture cross section [47, 49, 71].

Substituting Eq. (3-8) in Eq. (3-12):

$$\text{MACS} = \frac{2}{\sqrt{\pi}} \frac{1}{(kT)^2} A^{1.4} \, e^{-b \left[ \frac{2(N-Z)+1}{A} - \frac{(N+1-Z)^2}{A^2} \right]} \int_0^\infty a \, E_n \, e^{\left( \frac{-E_n}{kT} \right)} dE_n \tag{3-13}$$

$$\text{MACS} = \frac{2}{\sqrt{\pi}} \frac{1}{(kT)^2} A^{1.4} \, e^{-b \left[\frac{2(N-Z)+1}{A} - \frac{(N+1-Z)^2}{A^2}\right]} \frac{1.385 \times 10^{-4}}{g m_n c^2} \left(24t^4 + \frac{1375.2}{E_{GDR}^2} t^6\right)$$

$$\int_0^\infty e^{(c_1 + E_n - E_0)/t} \, e^{\left(\frac{-E_n}{kT}\right)} dE_n \tag{3-14}$$

Integrating the Eq. (3-14):

$$\text{MACS} = \frac{2}{\sqrt{\pi}} \frac{1}{(kT)^2} A^{1.4} \, e^{-b \left[\frac{2(N-Z)+1}{A} - \frac{(N+1-Z)^2}{A^2}\right]} \frac{1.385 \times 10^{-4}}{g m_n c^2} \left(24t^4 + \frac{1375.2}{E_{GDR}^2} t^6\right) e^{(c_1 - E_0)/t} \frac{tkT}{t-kT} \tag{3-15}$$

Defining the parameter **C** (in millibarn units) and $\frac{(N+1-Z)^2}{A^2} \sim \frac{(N-Z)^2}{A^2}$ :

$$C = \frac{2}{\sqrt{\pi}} \frac{1}{kT} \frac{1.385 \times 10^{-4}}{g m_n c^2} \left(24t^4 + \frac{1375.2}{E_{GDR}^2} t^6\right) e^{(c_1 - E_0)/t} \frac{t}{t-kT} \, e^{-b\left[\frac{2(N-Z)+1}{A}\right]} \quad \textbf{(mb)} \tag{3-16}$$

the **MACS (Z,A)** is reduced to:

$$\text{MACS (Z, A)} = C \, A^{1.4} \, e^{b\left[\frac{(N-Z)^2}{A^2}\right]} \tag{3-17}$$

Applying logarithms the Eq. (3-17) is reduced to:

$$\log_{10}\left(\frac{\text{MACS(Z,A)}}{A^{1.4}}\right) = \frac{b}{\ln(10)} \left[\frac{(N-Z)^2}{A^2}\right] + \log_{10} C \tag{3-18}$$

Eq. (3-18) is a linear function in the form **Y = A X + B**, with $A = \frac{b}{\ln(10)}$ and $B = \log_{10} C$. This equation contains two parameters (**C** and **b**) to be determined with the least squares adjustment method.

*Table 3.1* presents the experimental Maxwellian Averaged Cross Sections (MACS) at 30 keV for 89 isotopes for 15 elements with mass number $70 \le A \le 204$. The MACS values adopted in this study were taken from the KADoNis database (KADoNis 2023). A significant number of nuclei, have limited experimental data available, often consisting of less than three isotopes for odd-A or

even-A nuclei. Having at least three isotopes is important for conducting a reliable fit and accurately assessing the linear dependency.

**Table 3.1.** Experimental MACS at 30 keV for nuclei along different isotopic chains from KADoNiS database [70].

| Z | A | | MACS $_{exp}$ (mb) | ΔMACS $_{exp}$ (mb) | Ref. |
|---|---|---|---|---|---|
| 32 (Ge) | Even | 70 | 88.0 | 5.0 | [49] |
| | | 72 | 73.0 | 7.0 | [49] |
| | | 74 | 37.6 | 3.9 | [72] |
| | | 76 | 21.5 | 1.8 | [72] |
| 34 (Se) | Even | 74 | 271.0 | 15.0 | [73] |
| | | 76 | 164.0 | 8.0 | [49, 74] |
| | | 78 | 60.1 | 9.6 | [75] |
| | | 80 | 42.0 | 3.0 | [49] |
| | | 82 | 9.0 | 8.0 | [49] |
| 36 (Kr) | Odd | 79 | 959.0 | 162.0 | [49] |
| | | 81 | 607.0 | 105.0 | [49] |
| | | 83 | 243.0 | 15.0 | [49] |
| | | 85 | 55.0 | 45.0 | [49] |
| | Even | 78 | 321.0 | 26.0 | [49] |
| | | 80 | 267.0 | 14.0 | [49] |
| | | 82 | 90.0 | 6.0 | [49] |
| | | 84 | 38.0 | 4.0 | [49] |
| 50 (Sn) | Odd | 115 | 342.4 | 8.7 | [49, 76] |
| | | 117 | 318.8 | 4.8 | [49, 76] |
| | | 119 | 180.0 | 10.0 | [49] |
| | | 121 | 167.0 | 30.0 | [49] |
| | | 125 | 59.0 | 9.0 | [49] |
| | Even | 112 | 210.0 | 12.0 | [49] |
| | | 114 | 134.4 | 1.8 | [49, 76] |
| | | 116 | 91.6 | 0.6 | [77] |
| | | 118 | 62.1 | 0.6 | [49] |
| | | 120 | 36.2 | 0.3 | [77] |
| | | 122 | 21.9 | 1.5 | [49] |

| | | 124 | 12.0 | 1.8 | [49] |
|---|---|---|---|---|---|
| | | 126 | 10.0 | 4.0 | [49] |
| **51 (Sb)** | **Odd** | 121 | 532.0 | 16.0 | [49, 78] |
| | | 123 | 303.0 | 9.0 | [49, 78] |
| | | 125 | 260.0 | 70.0 | [49] |
| **52 (Te)** | **Even** | 120 | 538.0 | 26.0 | [49] |
| | | 122 | 295.0 | 3.0 | [49] |
| | | 124 | 155.0 | 2.0 | [49] |
| | | 126 | 81.3 | 1.4 | [49, 79] |
| | | 128 | 44.4 | 1.3 | [49, 78] |
| | | 130 | 14.7 | 2.8 | [49] |
| **54 (Xe)** | **Odd** | 129 | 617.0 | 12.0 | [80] |
| | | 131 | 340.0 | 65.0 | [49] |
| | | 133 | 127.0 | 34.0 | [49] |
| | **Even** | 124 | 644.0 | 83.0 | [49, 81] |
| | | 126 | 359.0 | 51.0 | [49, 81] |
| | | 128 | 262.5 | 3.7 | [80] |
| | | 130 | 132.0 | 2.1 | [80] |
| | | 132 | 64.6 | 5.3 | [49, 81] |
| | | 134 | 20.2 | 1.7 | [49, 81] |
| **56 (Ba)** | **Even** | 130 | 746.0 | 34.0 | [49] |
| | | 132 | 397.0 | 16.0 | [49] |
| | | 134 | 176.0 | 5.6 | [49] |
| | | 136 | 61.2 | 2.0 | [49] |
| **58 (Ce)** | **Odd** | 133 | 2600.0 | 400.0 | [49] |
| | | 135 | 1320.0 | 260.0 | [49] |
| | | 137 | 973.0 | 256.0 | [49] |
| | | 139 | 214.0 | 120.0 | [49] |
| | | 141 | 76.0 | 33.0 | [49] |
| | **Even** | 132 | 1570.0 | 420.0 | [49] |
| | | 134 | 967.0 | 351.0 | [49] |
| | | 136 | 328.0 | 21.0 | [49, 82] |
| | | 138 | 179.0 | 5.0 | [49, 82] |
| | | 142 | 28.0 | 1.0 | [49] |
| **63 (Eu)** | **Odd** | 151 | 3478.0 | 77.0 | [83] |
| | | 153 | 2556.0 | 46.0 | [83] |

| | | 155 | 1320.0 | 84.0 | [49, 84] |
|---|---|---|---|---|---|
| **64 (Gd)** | **Odd** | 153 | 4550.0 | 700.0 | [49] |
| | | 155 | 2648.0 | 30.0 | [85] |
| | | 157 | 1369.0 | 15.0 | [85] |
| **68 (Er)** | **Even** | 162 | 1624.0 | 124.0 | [49] |
| | | 164 | 1084.0 | 51.0 | [49, 83] |
| | | 166 | 563.0 | 56.0 | [49] |
| | | 168 | 338.0 | 44.0 | [49] |
| | | 170 | 170.0 | 7.0 | [49] |
| **70 (Yb)** | **Odd** | 171 | 1210.0 | 12.0 | [49, 86, 87] |
| | | 173 | 754.0 | 7.0 | [49] |
| | | 175 | 558.0 | 83.0 | [49] |
| **78 (Pt)** | **Even** | 190 | 508.0 | 44.0 | [88] |
| | | 192 | 590.0 | 120.0 | [49] |
| | | 194 | 365.0 | 85.0 | [49] |
| | | 196 | 183.0 | 16.0 | [49] |
| | | 198 | 92.2 | 4.6 | [49] |
| **80 (Hg)** | **Odd** | 199 | 374.0 | 23.0 | [49, 89] |
| | | 201 | 264.0 | 14.0 | [49, 89] |
| | | 203 | 98.0 | 17.0 | [49] |
| | **Even** | 196 | 204.0 | 8.0 | [88] |
| | | 198 | 173.0 | 15.0 | [49, 89] |
| | | 200 | 115.0 | 12.0 | [49, 89] |
| | | 202 | 63.2 | 1.9 | [49] |
| | | 204 | 42.0 | 4.0 | [49, 89] |

The investigation is focused on studying the behavior of MACS for nuclei along various isotopic chains. These isotopic chains were selected based on the availability of experimental data. It's worth noting that the selection was limited to the existing data, as the accuracy and reliability of MACS calculations heavily rely on the availability of experimental measurements. In order to gain a deeper understanding of the MACS behavior along different isotopic chains, future studies could explore the possibility of expanding the available experimental data. By incorporating newly acquired MACS measurements, researchers can further refine their investigations and enhance the accuracy of their predictions.

Furthermore, the proposed formula, referred to as Eq. (3-12), holds promise for future investigations. This formula, when applied to the analysis of MACS data, has the potential to provide valuable insights into the underlying nuclear processes. However, it's important to note that the formula's effectiveness and validity can only be fully assessed through rigorous testing and verification using experimental data. Given the dynamic nature of scientific research, it's reasonable to anticipate that additional MACS data will become available in the future. The incorporation of such data into analyses and calculations would undoubtedly contribute to expanding our knowledge and refining our understanding of nuclear reactions [90].

***Figure 3.1*** shows the values of the $\frac{MACS}{A^{1.4}}$ as a function of $\frac{(N-Z)^2}{A^2}$, for the nuclei present in ***Table 3.1*** [90].
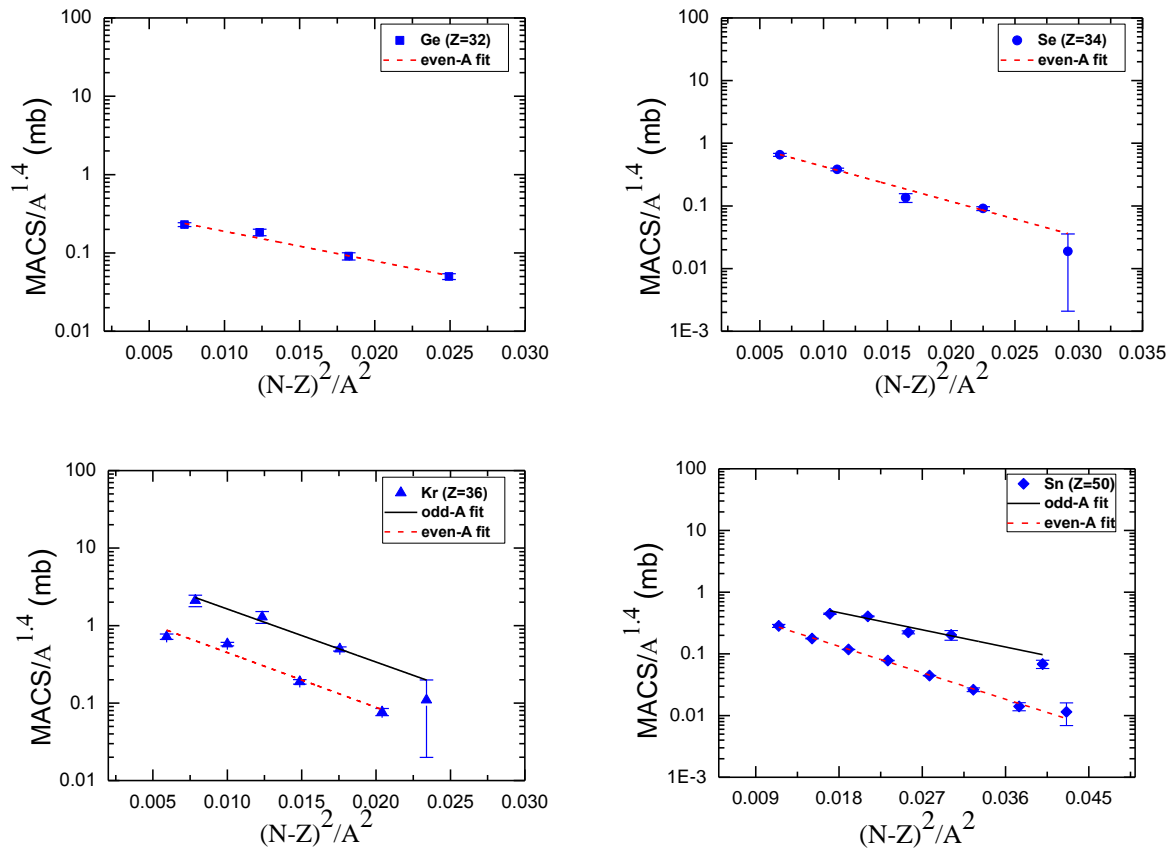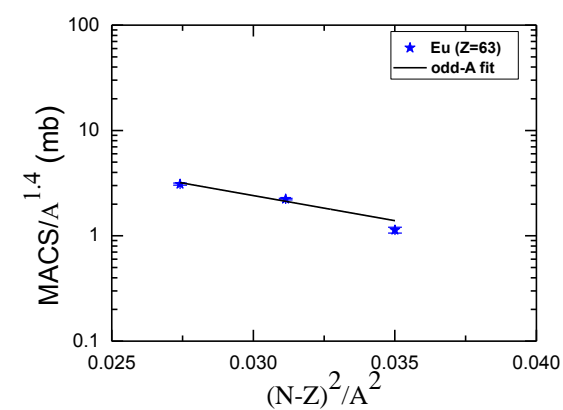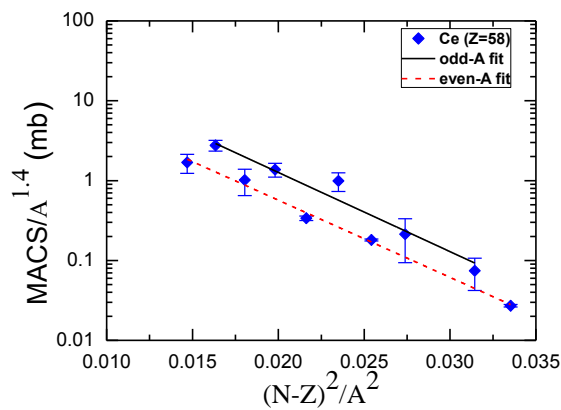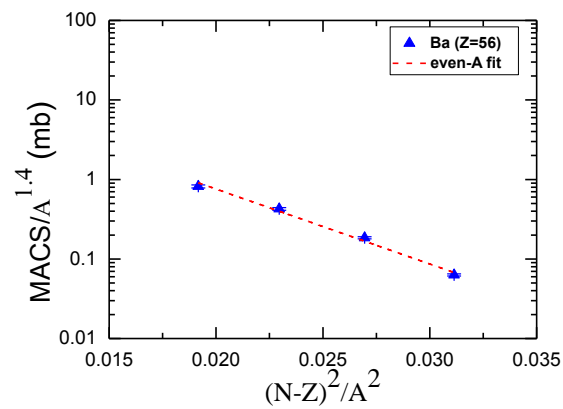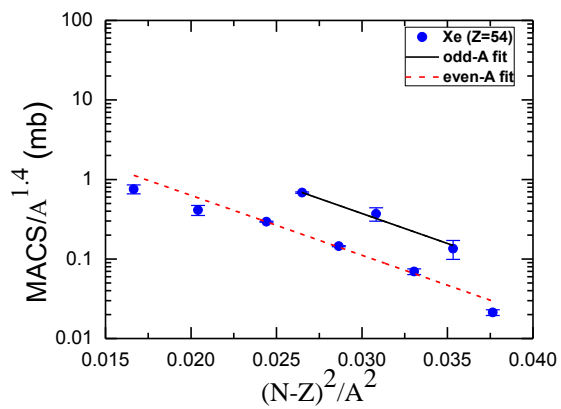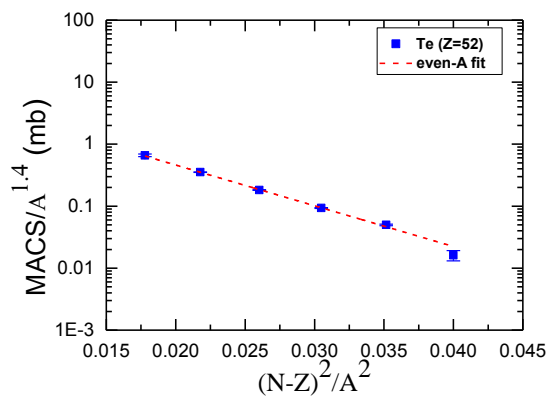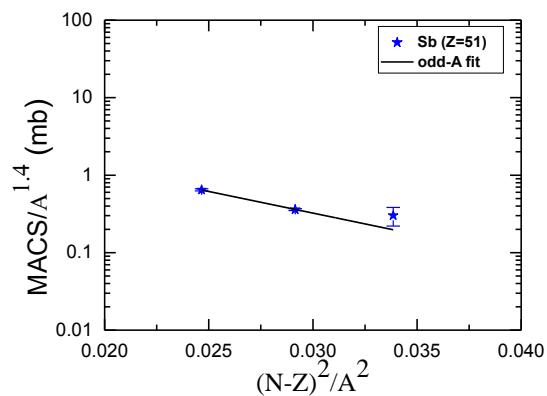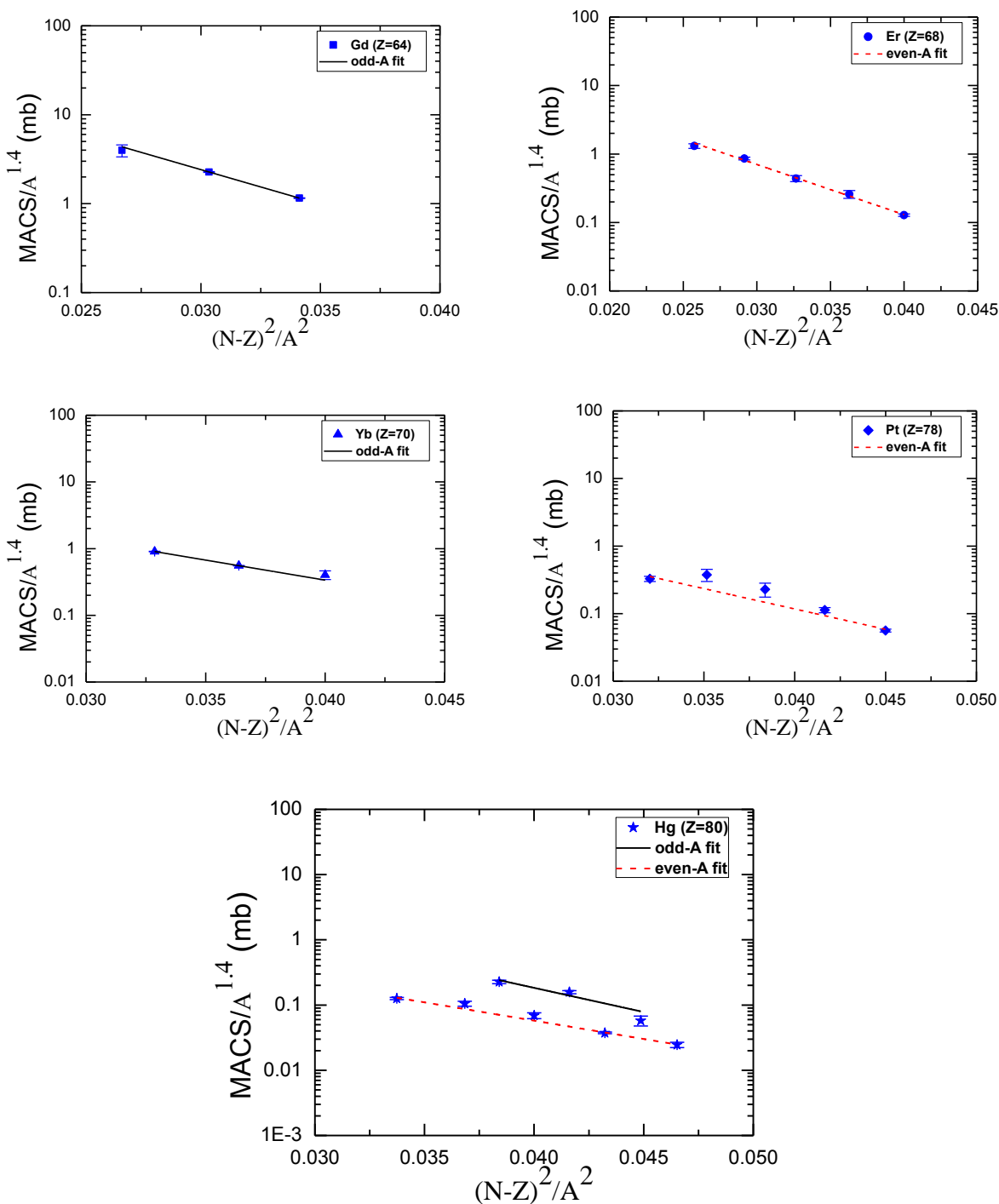
**Figure 3.1.** The $\frac{MACS}{A^{1.4}}$ values as a function of $\frac{(N-Z)^2}{A^2}$ for nuclei along different isotopic chains [90].

Upon careful examination of ***Figure 3.1***, it becomes evident that a linear dependence can be observed for both odd-A and even-A nuclei, particularly where A, representing the mass number, is significantly greater than 1. This finding suggests the presence of a systematic relationship between the $\frac{\text{MACS}}{A^{1.4}}$ values and the $\frac{(N-Z)^2}{A^2}$ ratio.

To further elucidate the observed trends, the figure includes two distinct lines: a solid line and a dashed line. These lines are constructed based on the least-$\chi^2$ fits of the experimental MACS, which are represented on a logarithmic scale. The fitting process follows Eq. (3-18). The solid line and dashed line visually represent the best-fit curves obtained through this fitting procedure. By comparing the positions and trajectories of the fitted lines with the data points, one can evaluate the degree to which the model accurately captures the underlying relationship.

It's worth noting that the fitting procedure employed here aims to minimize the discrepancy between the experimental MACS values and the values predicted by Eq. (3-18). The least-$\chi^2$ criterion is utilized as a measure of the overall agreement between the model and the data, ensuring a rigorous assessment of the fitting quality. By selecting the parameters that minimize the $\chi^2$ value, the best-fit curves are obtained [90].

## 4. Results and discussion

### 4.1. Fitting of systematics parameters

The best fit corresponds to the minimum of the following expression [91]:

$$\chi^2 = \frac{\Sigma}{(N-M)} = \frac{1}{(N-M)} \sum_{i=1}^{N} \left( \frac{\sigma_i^{exp} - \sigma_i^{cal}}{\Delta\sigma_i^{exp}} \right)^2 \qquad \textbf{(3-13)}$$

The quantity $\boldsymbol{\chi^2}$, known as the reduced Chi-squared, is a statistical criterion to assert the accuracy of a given analytical model or formula. The quantity $\boldsymbol{\Sigma}$ gives the weighted deviation of the calculated data $\boldsymbol{\sigma_i^{cal}}$ from the experimental ones given by $\boldsymbol{\sigma_i^{exp}}$ and $\Delta\boldsymbol{\sigma_i^{exp}}$, where $\mathbf{N}$ is the number of experimental data points and $\mathbf{M}$ is the number of fitting parameters (constraints) [91].

The obtained values of the fitting parameters C and b, and the values for $\Sigma$ and $\chi^2$ are listed in **Table 3.2**. The values of $\chi^2$ are small for most elements, which suggests Eq. (3-18) would be helpful to estimate the MACS of neighboring isotopes for which no experimental data are available [90].

**Table 3.2.** Obtained values of the parameters C and b, and the corresponding

$\Sigma$ and $\chi^2$ values of the fits [90].

| Z | Type of nuclei | C (mb) | b | $\Sigma$ | $\chi^2$ |
|---|---|---|---|---|---|
| 32 (Ge) | Even-A | 0.44 ± 0.04 | -87.08 ± 6.92 | 3.29 | 1.64 |
| 34 (Se) | Even-A | 1.53 ± 0.18 | -128.66 ± 9.08 | 7.87 | 2.62 |
| 36 (Kr) | Odd-A | 7.91 ± 1.93 | -157.68 ± 14.92 | 1.77 | 0.88 |
| | Even-A | 2.28 ± 0.78 | -162.96 ± 26.93 | 26.87 | 13.43 |
| 50 (Sn) | Odd-A | 1.68 ± 0.64 | -71.30 ± 18.40 | 73.88 | 24.62 |
| | Even-A | 0.95 ± 0.05 | -109.62 ± 2.38 | 36.9 | 6.15 |
| 51 (Sb) | Odd-A | 15.30 ± 4.99 | -128.50 ± 12.06 | 1.69 | 1.69 |
| 52 (Te) | Even-A | 9.47 ± 0.71 | -151.32 ± 2.98 | 12.29 | 3.07 |
| 54 (Xe) | Odd-A | 68.12 ± 32.81 | -173.56 ± 18.10 | 0.54 | 0.54 |
| | Even-A | 20.20 ± 6.09 | -173.44 ± 11.32 | 48.62 | 12.15 |
| 56 (Ba) | Even-A | 58.11 ± 20.60 | -217.06 ± 13.33 | 21.80 | 10.90 |
| 58 (Ce) | Odd-A | 121.62 ± 56.61 | -228.28 ± 23.12 | 3.15 | 1.05 |
| | Even-A | 48.59 ± 12.43 | -222.54 ± 9.12 | 12.41 | 4.13 |
| 63 (Eu) | Odd-A | 64.71 ± 55.34 | -109.68 ± 28.53 | 22.42 | 22.42 |
| 64 (Gd) | Odd-A | 519.38 ± 43.93 | -179.05 ± 2.61 | 0.40 | 0.40 |
| 68 (Er) | Even-A | 111.29 ± 19.19 | -168.85 ± 5.00 | 3.43 | 1.14 |
| 70 (Yb) | Odd-A | 85.59 ± 12.87 | -138.45 ± 4.32 | 1.27 | 1.27 |
| 78 (Pt) | Even-A | 30.05 ± 17.65 | -138.71 ± 14.04 | 11.67 | 3.89 |
| 80 (Hg) | Odd-A | 169.31 ± 418.81 | -170.68 ± 61.08 | 10.71 | 10.71 |
| | Even-A | 10.16 ± 3.04 | -129.36 ± 7.44 | 7.37 | 2.45 |

The ability to estimate the MACS of neighboring isotopes is particularly significant in cases where experimental data is scarce or not obtainable. Eq. (3-18), based on the obtained fitting

parameters C and b, provides a means to approximate the MACS values for these isotopes. By leveraging the well-defined relationship captured by the fitted function, researchers can extrapolate and predict the behavior of neighboring isotopes that have not been directly measured [90].

### 4.2. Comparison between calculated data and experimental data

The values of the MACS calculated with the proposed formula (Eq. 3-17) were compared with the experimental ones from the KADoNis database. The ratio $\frac{MACS\ exp}{MACS\ cal}$ and relative error was also determined and the results are summarized in ***Table 3.3*** [90].

**Table 3.3.** Ratio between the experimental and calculated MACS at 30 keV [90].

| Z | A | | MACS $_{exp}$ ± ΔMACS $_{exp}$ (mb) | MACS $_{cal}$ (mb) | $\dfrac{MACS\ exp}{MACS\ cal}$ | $\dfrac{\lvert MACS\ exp - MACS\ cal\rvert}{MACS\ exp} \times 100$ (%) |
|---|---|---|---|---|---|---|
| **32 (Ge)** | **Even** | 70 | 88.00 ± 5.00 | 88.87 | 0.99 | 0.98 |
| | | 72 | 73.00 ± 7.00 | 59.82 | 1.22 | 18.05 |
| | | 74 | 37.60 ± 3.90 | 37.13 | 1.01 | 1.25 |
| | | 76 | 21.50 ± 1.80 | 21.57 | 1.00 | 0.32 |
| **34 (Se)** | **Even** | 74 | 271.00 ± 15.00 | 271.82 | 1.00 | 0.30 |
| | | 76 | 164.00 ± 8.00 | 158.02 | 1.04 | 3.64 |
| | | 78 | 60.10 ± 9.60 | 82.26 | 0.73 | 36.87 |
| | | 80 | 42.00 ± 3.00 | 39.07 | 1.08 | 6.97 |
| | | 82 | 9.00 ± 8.00 | 17.19 | 0.52 | 91.00 |
| **36 (Kr)** | **Odd** | 79 | 959.00 ± 162.00 | 1040.00 | 0.92 | 8.44 |
| | | 81 | 607.00 ± 105.00 | 530.40 | 1.14 | 12.61 |
| | | 83 | 243.00 ± 15.00 | 241.00 | 1.01 | 0.82 |
| | | 85 | 55.00 ± 45.00 | 99.44 | 0.55 | 80.80 |
| | **Even** | 78 | 321.00 ± 26.00 | 387.30 | 0.83 | 20.65 |
| | | 80 | 267.00 ± 14.00 | 206.30 | 1.29 | 22.73 |
| | | 82 | 90.00 ± 6.00 | 96.55 | 0.93 | 7.27 |
| | | 84 | 38.00 ± 4.00 | 40.51 | 0.94 | 6.60 |

| | | | | | |
|---|---|---|---|---|---|
| **50 (Sn)** | **Odd** | 115 | 342.40 ± 8.70 | 383.20 | 0.89 | 11.91 |
| | | 117 | 318.80 ± 4.80 | 293.10 | 1.09 | 8.06 |
| | | 119 | 180.00 ± 10.00 | 219.60 | 0.82 | 22.00 |
| | | 121 | 167.00 ± 30.00 | 161.60 | 1.03 | 3.23 |
| | | 125 | 59.00 ± 9.00 | 83.63 | 0.71 | 41.74 |
| | **Even** | 112 | 210.00 ± 12.00 | 199.58 | 1.05 | 4.96 |
| | | 114 | 134.40 ± 1.80 | 137.85 | 0.98 | 2.56 |
| | | 116 | 91.60 ± 0.60 | 91.67 | 0.99 | 0.07 |
| | | 118 | 62.10 ± 0.60 | 58.96 | 1.05 | 5.05 |
| | | 120 | 36.20 ± 0.30 | 36.83 | 0.98 | 1.74 |
| | | 122 | 21.90 ± 1.50 | 22.41 | 0.98 | 2.32 |
| | | 124 | 12.00 ± 1.80 | 13.34 | 0.90 | 11.16 |
| | | 126 | 10.00 ± 4.00 | 7.78 | 1.29 | 22.2 |
| **51 (Sb)** | **Odd** | 121 | 532.00 ± 16.00 | 530.40 | 1.00 | 0.30 |
| | | 123 | 303.00 ± 9.00 | 304.70 | 0.99 | 0.56 |
| | | 125 | 260.00 ± 70.00 | 170.2 | 1.53 | 34.53 |
| **52 (Te)** | **Even** | 120 | 538.00 ± 26.00 | 523.50 | 1.03 | 2.69 |
| | | 122 | 295.00 ± 3.00 | 292.90 | 1.01 | 0.71 |
| | | 124 | 155.00 ± 2.00 | 157.60 | 0.98 | 1.67 |
| | | 126 | 81.30 ± 1.40 | 81.92 | 0.99 | 0.76 |
| | | 128 | 44.40 ± 1.30 | 41.31 | 1.07 | 6.95 |
| | | 130 | 14.70 ± 2.80 | 20.28 | 0.72 | 37.95 |
| **54 (Xe)** | **Odd** | 129 | 617.00 ± 12.00 | 617.41 | 0.99 | 0.06 |
| | | 131 | 340.00 ± 65.00 | 297.80 | 1.14 | 12.41 |
| | | 133 | 127.00 ± 34.00 | 139.13 | 0.91 | 9.55 |
| | **Even** | 124 | 644.00 ± 83.00 | 959.50 | 0.67 | 48.99 |
| | | 126 | 359.00 ± 51.00 | 511.30 | 0.70 | 42.42 |
| | | 128 | 262.50 ± 3.70 | 260.90 | 1.01 | 0.60 |
| | | 130 | 132.00 ± 2.10 | 128.10 | 1.03 | 2.95 |
| | | 132 | 64.60 ± 5.30 | 60.83 | 1.06 | 5.83 |
| | | 134 | 20.2 ± 1.70 | 28.02 | 0.72 | 38.71 |
| **56 (Ba)** | **Even** | 130 | 746.00 ± 34.00 | 825.10 | 0.90 | 10.60 |
| | | 132 | 397.00 ± 16.00 | 370.60 | 1.07 | 6.64 |
| | | 134 | 176.00 ± 5.60 | 158.9 | 1.11 | 9.71 |
| | | 136 | 61.20 ± 2.00 | 65.39 | 0.94 | 6.84 |
| | | 133 | 2600.00 ± 400.00 | 2746.00 | 0.95 | 5.61 |

| | | | | | |
|---|---|---|---|---|---|
| | **Odd** | 135 | 1320.00 ± 260.00 | 1270.00 | 1.04 | 3.78 |
| | | 137 | 973.00 ± 256.00 | 558.40 | 1.74 | 42.61 |
| | | 139 | 214.00 ± 120.00 | 234.90 | 0.91 | 9.76 |
| **58 (Ce)** | | 141 | 76.00 ± 33.00 | 94.89 | 0.8 | 24.85 |
| | **Even** | 132 | 1570.00 ± 420.00 | 1719.00 | 0.91 | 9.49 |
| | | 134 | 967.00 ± 351.00 | 832.90 | 1.16 | 13.86 |
| | | 136 | 328.00 ± 21.00 | 383.10 | 0.86 | 16.79 |
| | | 138 | 179.00 ± 5.00 | 168.30 | 1.06 | 5.97 |
| | | 142 | 28.00 ± 1.00 | 28.82 | 0.97 | 2.92 |
| | **Odd** | 151 | 3478.00 ± 77.00 | 3596.00 | 0.97 | 3.39 |
| **63 (Eu)** | | 153 | 2556.00 ± 46.00 | 2433.00 | 1.05 | 4.81 |
| | | 155 | 1320.00 ± 84.00 | 1622.00 | 0.81 | 22.87 |
| | **Odd** | 153 | 4550.00 ± 700.00 | 4987.90 | 0.91 | 9.62 |
| **64 (Gd)** | | 155 | 2648.00 ± 30.00 | 2645.05 | 1.00 | 0.11 |
| | | 157 | 1369.00 ± 15.00 | 1369.73 | 0.99 | 0.05 |
| | **Even** | 162 | 1624.00 ± 124.00 | 1782.00 | 0.91 | 9.72 |
| | | 164 | 1084.00 ± 51.00 | 1023.00 | 1.06 | 5.62 |
| **68 (Er)** | | 166 | 563.00 ± 56.00 | 574.90 | 0.98 | 2.11 |
| | | 168 | 338.00 ± 44.00 | 317.20 | 1.07 | 6.15 |
| | | 170 | 170.00 ± 7.00 | 172.10 | 0.99 | 1.23 |
| | **Odd** | 171 | 1210.00 ± 12.00 | 1209.26 | 1.00 | 0.06 |
| **70 (Yb)** | | 173 | 754.00 ± 7.00 | 754.85 | 0.99 | 0.11 |
| | | 175 | 558.00 ± 83.00 | 465.11 | 1.20 | 16.64 |
| | **Even** | 190 | 508.00 ± 44.00 | 548.30 | 0.93 | 7.93 |
| | | 192 | 590.00 ± 120.00 | 360.30 | 1.64 | 38.93 |
| **78 (Pt)** | | 194 | 365.00 ± 85.00 | 234.10 | 1.56 | 35.86 |
| | | 196 | 183.00 ± 16.00 | 150.70 | 1.21 | 17.65 |
| | | 198 | 92.20 ± 4.60 | 96.07 | 0.96 | 4.19 |
| | **Odd** | 199 | 374.00 ± 23.00 | 398.16 | 0.94 | 6.45 |
| | | 201 | 264.00 ± 14.00 | 233.86 | 1.13 | 11.41 |
| | | 203 | 98.00 ± 17.00 | 135.91 | 0.72 | 38.68 |
| **80 (Hg)** | **Even** | 196 | 204.00 ± 8.00 | 209.30 | 0.97 | 2.59 |
| | | 198 | 173.00 ± 15.00 | 142.20 | 1.22 | 17.80 |
| | | 200 | 115.00 ± 12.00 | 95.75 | 1.20 | 16.73 |
| | | 202 | 63.20 ± 1.90 | 63.92 | 0.99 | 1.13 |
| | | 204 | 42.00 ± 4.00 | 42.35 | 0.99 | 0.83 |

The objective of this study is to analyze the relationship between the experimental and calculated Maxwellian Averaged Cross Sections (MACS) as a function of the mass number (A). To visualize this relationship, ***Figure 3.2*** displays a plot illustrating the ratio between the experimental and calculated MACS values [90].
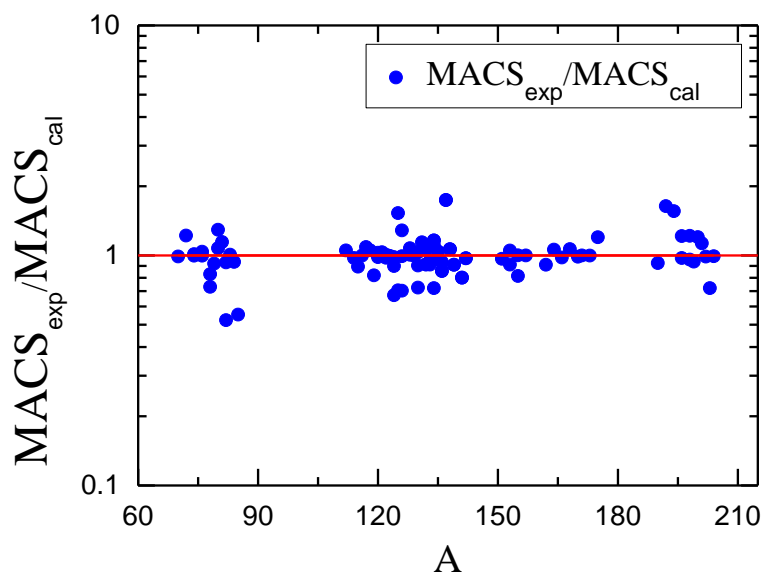


**Figure 3.2.** Ratio between the experimental and calculated (Eq. 3-17) MACS values as a function the mass numbers A [90].

Upon observing ***Figure 3.2***, it becomes evident that the majority of nuclei exhibit a ratio very close to unity. This implies a substantial level of agreement between the experimental and calculated MACS values. Such agreement is indicative of a reliable and accurate calculation method utilized in this study.

Conversely, the fact that the majority of nuclei demonstrate a ratio very close to unity suggests a robust physics basis for Eq. (3-18). Eq. (3-18) serves as a mathematical representation employed in this study to describe the MACS along different isotopic chains. The consistency observed between the experimental and calculated MACS values provides compelling evidence

supporting the validity and applicability of Eq. (3-18) in describing the behavior of MACS across a wide range of isotopic chains [90].

## 5. Conclusion

The findings from this study hold significant implications for the field of nuclear physics. The strong agreement between experimental and calculated MACS values implies that the calculation method employed in this study captures the essential physical phenomena governing the MACS behavior. Consequently, this study contributes to the advancement of our fundamental understanding of nuclear reactions and their underlying mechanisms.

Furthermore, the systematic approach developed in this study proves to be highly useful for the analysis of experimental data. The systematic framework implemented allows for a comprehensive and rigorous examination of the experimental results. By comparing the experimental MACS values with the corresponding calculated values, researchers gain valuable insights into the accuracy of the theoretical models employed in the calculation process.

In conclusion, this study demonstrates a remarkable agreement between experimental and calculated MACS values for a wide range of nuclei. The observed ratio very close to unity indicates a strong concordance between the two sets of values, validating the physics basis of Eq. (3-18) in describing MACS behavior across different isotopic chains. The systematic approach developed in this study proves to be a valuable tool for the comprehensive analysis of experimental data. The findings of this study contribute to our understanding of nuclear reactions, and have significant implications for various scientific and technological applications [90].

# General Conclusion

# *General Conclusion*

This research focused on studying the systematics of Maxwellian Averaged Neutron Capture Cross Sections (MACS) at 30 keV for various isotopic chains, including both odd-A and even-A nuclei with A ≫ 1. The MACS plays a crucial role in nuclear astrophysics and understanding its behavior is essential for accurate predictions and data analysis.

The study proposed a formula to predict MACS values for different isotopic chains at 30 keV. The predictions obtained from this formula were compared with experimental data, and a substantial level of agreement was found between most of the predictions and the corresponding experimental measurements. This agreement suggests that the proposed systematic law is valuable in analyzing experimental data and provides a useful tool for quickly estimating MACS values with relatively good precision.

However, the research acknowledged that the isotopic chains studied were limited by the available experimental data. To further validate and refine the systematic law, additional experimental data on MACS are needed, particularly in the region of unstable nuclei. Gathering more experimental data will allow for further testing of the proposed systematic law and enhance its applicability across a broader range of isotopic chains.

The research findings demonstrate significant accomplishments in understanding the systematics of MACS at 30 keV for different isotopic chains. The proposed formula shows favorable agreement with experimental data, indicating its potential as a reliable tool for rapidly estimating MACS values with reasonable precision. The research outcomes have practical implications in various fields such as nuclear astrophysics, where knowledge of MACS is crucial.

The ability to accurately predict and describe MACS is of paramount importance in various applications, including nuclear energy generation, astrophysics, and medical applications. Understanding the behavior of MACS across different isotopic chains facilitates the development of more efficient and reliable nuclear energy systems. Moreover, this knowledge is crucial in the study of stellar nucleosynthesis processes, which are responsible for the synthesis of elements in stars. Additionally, in the field of medical physics, accurate MACS values are essential for radiation therapy treatment planning and dose calculations.

In conclusion, this research has made noteworthy progress in studying the systematics of MACS at 30 keV for different isotopic chains, encompassing odd-A and even-A nuclei with A $\gg$ 1. The proposed formula exhibit good agreement with experimental data, suggesting their usefulness in analyzing experimental results and estimating MACS values. However, the limited experimental data for certain isotopic chains, particularly in the region of unstable nuclei, emphasize the need for additional experimental efforts to validate and refine the systematic law. Expanding the experimental database will enhance the reliability and applicability of this systematic approach.

# Appendix

# *Appendix A*

Pictures taken at INFN-LNL (Istituto Nazionale di Fisica Nucleare-Laboratori Nazionali di Legnaro), Padova, Italy.
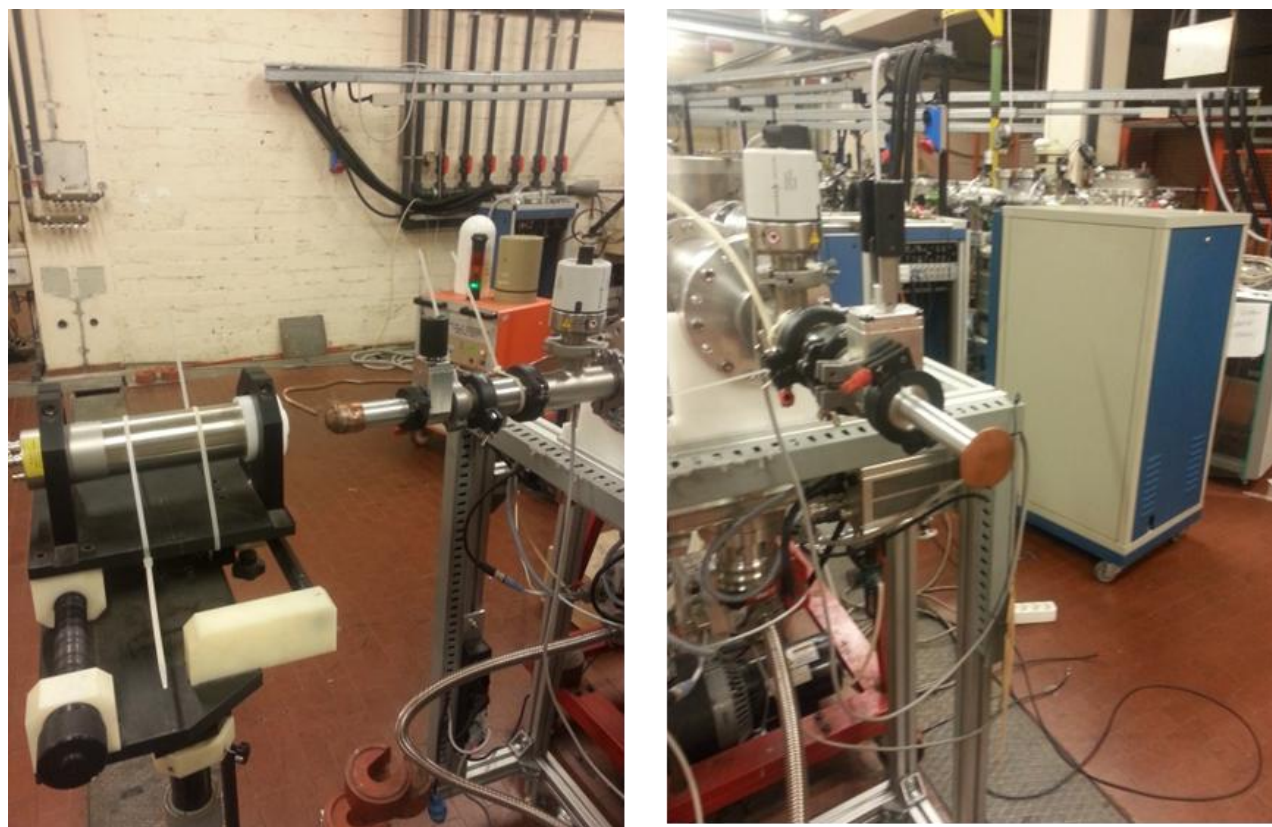


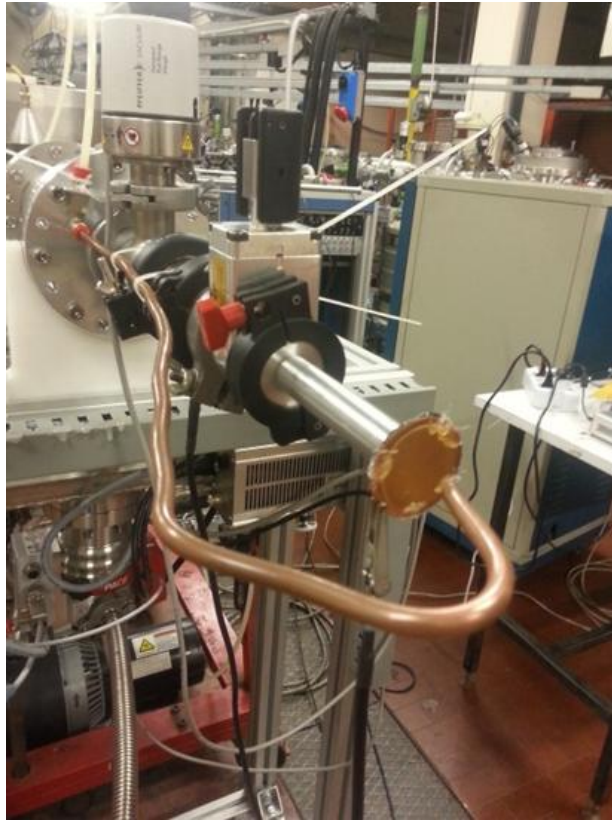**Figure A.1.** Generation of the neutron spectrum through the $^7$Li (p, n) $^7$Be reaction.

**Figure A.2.** Measuring of the MACS for $^{197}$Au(n, γ) at kT= 30 keV
by Activation.

# *Appendix B*

The KADoNiS (Karlsruhe Astrophysical Database of Nucleosynthesis in Stars) is an online database for Maxwellian Averaged (n,γ) Cross Sections.



**Figure B.1.** The main interface of KADoNiS.



**Figure B.2.** Example of introducing an element ($^{70}$Ge) in KADoNiS.

**Figure B.3.** The KADoNiS result interface.

# References

# *References*

[1] Dzysiuk, N., Mastinu, P., Martin, G., Praena, J., & Baraldo, A. (2010). A New Approach to Obtain a Maxwell-Boltzmann Neutron Spectrum at Different kT Within the LENOS Project. *Laboratori Nazionali di Legnaro Annual Report*, 125-126.

[2] Pritychenko, B., Mughaghab, S. F., & Sonzogni, A. A. (2010). Calculations of Maxwellian-averaged cross sections and astrophysical reaction rates using the ENDF/B-VII. 0, JEFF-3.1, JENDL-3.3, and ENDF/B-VI.8 evaluated nuclear reaction data libraries. *Atomic Data and Nuclear Data Tables*, *96*(6), 645-748.

[3] Abdullah, H. M., & Ahmed, A. H. (2022). Empirical formulae for (n, p) reaction cross-sections at 14–15 MeV neutrons. *International Journal of Modern Physics E*, *31*(05), 2250049.

[4] Broeders, C. H. M., & Konobeyev, A. Y. (2008). Systematics of (p, n) reaction cross-section. *Radiochimica Acta*, *96*(7), 387-397.

[5] Lyes, O., & Amrani, N. (2023). New semi-empirical systematic of (p, n) reaction cross section at 7.5 MeV. *Kerntechnik*, *88*(3), 279-290.

[6] Tel, E., Okuducu, Ş., Bölükdemir, M. H., & Tanir, G. (2008). Semi-empirical systematics of (n, 2n),(n, α) reactions cross sections at 14–15 MeV neutron energy. *International Journal of Modern Physics E*, *17*(03), 567-583.

[7] Yiğit, M. (2015). Empirical formula on (n, 3He) reaction cross sections at 14.6 MeV neutrons. *Applied Radiation and Isotopes*, *105*, 15-19.

[8] Yiğit, M. (2017). New empirical formulae for (n, t) cross sections at 14.6 MeV. *Applied Radiation and Isotopes*, *128*, 307-310.

[9] Yiğit, M. (2018). Analysis of (n, p) cross sections near 14 MeV. *Applied Radiation and Isotopes*, *135*, 115-122.

[10] Yiğit, M. (2020). Analysis of the reaction Q-value effect using newly evaluated empirical formulas of (n, 2 n) cross-sections near 14.6 MeV. *International Journal of Modern Physics E*, *29*(02), 2050005.

[11] Yiğit, M. (2020). A new empirical formula for cross-sections of (n, n α) reactions. *International Journal of Modern Physics E*, *29*(08), 2050062.

[12] Kiss, M., & Trócsányi, Z. (2013). Phenomenological description of neutron capture cross sections at 30 keV. *International Scholarly Research Notices*, *2013*(1), 170954.

[13] Krane, K. S. (1991). *Introductory nuclear physics*. John Wiley & Sons.

[14] Boucenna, A. (2017). *La Physique nucléaire*, Dar el Djazairia.

[15] Tesfaye, T. Physique nucléaire, Université Virtuelle Africaine Addis. Ababa, License (Creative Commons), Version 2.5.

[16] Arnoud, Y. (2011-2012). PHY113 : Cours de Radioactivité, Mise à jour en 2011 par Ingo Schienbein.

[17] Basdevant, J. L., Rich, J., & Spiro, M. (2002). *Energie nucléaire*. Editions Ecole Polytechnique.

[18] Reuss, P. (2003). *Précis de neutronique*, Ed, EDP sciences.

[19] Joob, N. Les Réactions Nucléaires Spontanées : La Radioactivité, CLASSE TS1.

[20] Sreepad, H.R. NUCLEAR REACTIONS, Lecture points, Govt College (Autonomous), Mandya.

[21] Erramli, H. (2017). Introduction à la physique nucléaire, Noor Publishing.

[22] Blanc, D. (1980). Physique Nucléaire, seconde édition, Edition Masson.

[23] Hamadani, H. M. T., Younis, T. A., & Ebrahiem, S. A. (2010). Evaluation of The Nuclear Data on (α, n) Reaction for Natural Molybdenum. *Ibn AL-Haitham Journal For Pure and Applied Science*, *23*(3), 76-85.

[24] Ducasse, Q. (2015). Etude de la méthode de substitution à partir de la mesure simultanée des probabilités de fission et d'émission gamma des actinides $^{236}$U, $^{238}$U, $^{237}$Np et $^{238}$Np. Thèse doctorat, Université de Bordeaux.

[25] Snow, W.M. neutron physics, Indiana University NPSS, Bar Harbor.

[26] Champion, C. Interaction des ondes et des particules avec la matière biologique. Laboratoire de Physique Moléculaire et des Collisions. Institut de Physique de Metz. Université de Metz.

[27] Benzaid, D. (2019). Caractérisation Théorique et Expérimentale d'un Spectromètre de Neutrons à Barrière de Surface, Thèse doctorat, UFAS.

[28] Puig, F., Dies, J. & Pereira, C. Multimédia de physique des réacteurs nucléaires Version 4.1. Nuclear Engineering Research Group. Departament de Fisica i Engeinyeria Nuclear,  EscolaTècnica Superior d'Enginyeria Industrial de Barcelona, Universitat Politècnica de Catalunya.

[29] Benmosbah, M. (2007). Spectrométrie des neutrons : étude de la réponse d'un ensemble de compteurs proportionnels. Thèse doctorat. École Doctorale Louis Pasteur. Université de Franche-Comté.

[30] Azbouche, A. Interaction des rayonnements avec la matière Théorie et applications. Formation continue et de perfectionnement. Centre de Recherche Nucléaire d'Alger (CRNA).

[31] Energy Deposition by Neutrons. (2006). Introduction to ionizing radiation fall, lecture notes, courses, nuclear engineering.

[32] Domanus, J. C. (Ed.). (1992). *Practical neutron radiography* (Vol. 16). Dordrecht: Kluwer Academic.

[33] Lferde, M. (1983). Détecteurs Solides de Traces et Neutronographie, thèse de doctorat Université Clermont-Ferrand II.

[34] Kadem, F. (2012). Détermination des sections efficaces d'activation des réactions nucléaires induites par neutrons et applications, thèse doctorat, USTHB.

[35] Lamarsh, J.R. (1983). Introducing to Nuclear Engineering, 2nd Edition, Addison-Wesley Company.

[36] Blanc, D. (1987). *Noyaux, particules, réacteurs nucléaires*. Paris: Masson.

[37] Boukerdja, L. (2016). Détermination des distributions spatiales et énergétiques des neutrons autour d'un réacteur nucléaire, thèse doctorat, UFAS 1.

[38] Belguet, S. (2016). Détermination d'une formule empirique pour les sections efficaces des réactions (n, p) à 14.5 MeV, mémoire de master, UFAS 1.

[39] Réaction nucléaire induite par le neutron. (2010). Sections efficaces neutrons, Paris-sud Université.

[40] Une équipe de physicien de DAM**. (2015). Les modèles de réactions nucléaires, CEA/DAM**.

[41] Slamene, H. (2009). Déperdition des neutrons par réactions non essentielles, Mémoire de Magister, UFAS1.

*References*

[42] Amrani, N. (2012). Radioactivité et Réactions Nucléaires. Cours de M1 Génie Physique Subatomique. Faculté des sciences. Université UFAS 1.

[43] Bertolloto, D., Epiney, A., & Girardin, G. (2007). *Mesures du Flux Neutronique par Spectrométrie γ et neutron* (Doctoral dissertation, PhD thesis, Ecole Polytechnique Fédérale de Lausanne-Suisse (Laboratoire de Physique des Réacteurs et de Comportement des Systèmes, EPFL-SB-IPEP-LRS, 2008)).

[44] Azizou, A. (2016). Développement d'un modèle semi-empirique pour calculer les sections efficaces des réactions nucléaires induites par les neutrons rapides, mémoire de master, UDBKM.

[45] Block, R. C., Danon, Y., Gunsing, F., & Haight, R. C. (2010). Neutron cross section measurements. In *Handbook of Nuclear Engineering*.

[46] Praena, J., Mastinu, P. F., & Hernández, G. M. (2009). A Method to Obtain a Maxwell–Boltzmann Neutron Spectrum at kT= 30 keV for Nuclear Astrophysics Studies. *Publications of the Astronomical Society of Australia*, *26*(3), 225-231.

[47] Rolfs, C.E. & Rodney, W.S. (1998). Cauldrons in the Cosmos. Nuclear Astrophysics, The University of Chicago Press.

[48] Bao, Z. Y., Beer, H., Käppeler, F., Voss, F., Wisshak, K., & Rauscher, T. (2000). Neutron cross sections for nucleosynthesis studies. *Atomic Data and Nuclear Data Tables*, *76*(1), 70-154.

[49] Martín-Hernández, G., Mastinu, P. F., Praena, J., Dzysiuk, N., Noy, R. C., & Pignatari, M. (2012). Temperature-tuned Maxwell–Boltzmann neutron spectra for kT ranging from 30 up to 50 keV for nuclear astrophysics studies. *Applied Radiation and Isotopes*, *70*(8), 1583-1589.

[50] Mastinu, P. F., Hernández, G. M., & Praena, J. (2009). A method to obtain a Maxwell–Boltzmann neutron spectrum at kT= 30 keV for nuclear astrophysics studies. *Nuclear Instruments*

*and Methods in Physics Research Section A: Accelerators, Spectrometers, Detectors and Associated Equipment*, *601*(3), 333-338.

[51] Dzysiuk, N., Mastinu, P., Martin, G., & Praena, J. (2009). Progress of the LENOS Project: Obtaining Maxwell-Boltzmann Distribution at kT=30 keV, LNL Annual Report.

[52] Reifarth, R., Heil, M., Käppeler, F., & Plag, R. (2009). PINO—a tool for simulating neutron spectra resulting from the $^7$Li(p, n) reaction. *Nuclear Instruments and Methods in Physics Research Section A: Accelerators, Spectrometers, Detectors and Associated Equipment*, *608*(1), 139-143.

[53] Praena, J., Mastinu, P. F., Pignatari, M., Quesada, J. M., Capote, R., & Morilla, Y. (2014). Measurement of the MACS of $^{159}$Tb(n, γ) at kT= 30 keV by Activation. *Nuclear Data Sheets*, *120*, 205-207.

[54] Lee, C. L., & Zhou, X. L. (1999). Thick target neutron yields for the $^7$Li (p, n) $^7$Be reaction near threshold. *Nuclear Instruments and Methods in Physics Research Section B: Beam Interactions with Materials and Atoms*, *152*(1), 1-11.

[55] Mastinu, P.F., Dzysiuk, N., Prete, G,. Capote Noy, R., Martín-Hernández, G., Pignatari, M., ... & Agostni, P. Present ans future of neutron beam line at LNL: BELINA and LENOS projects.

[56] Praena, J., Mastinu, P. F., Pignatari, M., Quesada, J. M., García-López, J., Lozano, M., ... & Martín-Hernández, G. (2013). Measurement of the MACS of $^{181}$Ta(n, γ) at kT= 30 keV as a test of a method for Maxwellian neutron spectra generation. *Nuclear Instruments and Methods in Physics Research Section A: Accelerators, Spectrometers, Detectors and Associated Equipment*, *727*, 1-6.

[57] Jimenez-Bonilla, P., & Praena, J. (2014). Measurement of the $^{197}$Au(n, γ) stellar cross section at kT= 30 keV by activation.

[58] Jiménez-Bonilla, P., Praena, J., & Quesada, J. M. (2018). Maxwellian Neutron Spectrum generation and Stellar Cross-Section measurements: measurement of the $^{197}$Au(n, γ) MACS. In *Journal of Physics: Conference Series* (Vol. 940, No. 1, p. 012044). IOP Publishing.

[59] Praena, J., & Jiménez-Bonilla, P. (2020). Two absolute integral measurements of the $^{197}$Au(n, γ) stellar cross-section and solution of the historic discrepancies. In *EPJ Web of Conferences* (Vol. 239, p. 19002). EDP Sciences.

[60] Martín-Hernández, G., Mastinu, P., Musacchio González, E., Capote, R., Lubián, H., & Macías, M. (2019). $^{7}$Li(*p, n*)$^{7}$Be cross section from threshold to 1960 keV and precise measurement of the $^{197}$Au(*n, γ*) spectrum-averaged cross section at 30 keV. *Physical Review C*, *99*(3), 034616.

[61] Djerboua, Y., Zhang, X., Amrani, N., Boucenna, A., & Ren, Z. (2015). Systematical law of (n, γ) reaction cross sections of odd-A nuclei. *Nuclear Physics A*, *938*, 14-21.

[62] Zhang, X. P., Li, G. W., Ren, Z. Z., Zheng, Q., Zhu, X. L., & Cheng, J. P. (2012). Systematical law of (n, γ) reaction cross sections of even-even nuclei. *Chinese Physics C*, *36*(3), 210.

[63] Borella, A., Gunsing, F., Moxon, M., Schillebeeckx, P., & Siegler, P. (2007). High-resolution neutron transmission and capture measurements of the nucleus $^{206}$Pb. *Physical Review C—Nuclear Physics*, *76*(1), 014605.

[64] Domingo-Pardo, C., Abbondanno, U., Aerts, G., Álvarez-Pol, H., Alvarez-Velarde, F., Andriamonje, S., ... & (n_TOF Collaboration). (2007). Measurement of the neutron capture cross section of the s-only isotope $^{204}$Pb from 1 eV to 440 keV. *Physical Review C—Nuclear Physics*, *75*(1), 015806.

[65] Krane, K. S., & Sylvester, J. (2006). Neutron capture cross sections of $^{112,116,122,124}$Sn. *Physical Review C—Nuclear Physics*, *73*(5), 054312.

*References*

[66] Noguere, G., Bouland, O., Brusegan, A., Schillebeeckx, P., Siegler, P., Lepretre, A., ... & Rudolf, G. (2006). Neutron capture and total cross sections of $^{127}$I and $^{129}$I. *Physical Review C—Nuclear Physics*, *74*(5), 054602.

[67] Forrest, R. A., Kopecky, J., & Koning, A. J. (2008). Revisions and improvements of neutron capture cross sections for EAF-2009 and validation of TALYS calculations. *UKAEA report UKAEA FUS*, *546*.

[68] Rauscher, T., Bieber, R., Oberhummer, H., Kratz, K. L., Dobaczewski, J., Möller, P., & Sharma, M. M. (1998). Dependence of direct neutron capture on nuclear-structure models. *Physical Review C*, *57*(4), 2031.

[69] Tao, C., Ma, Y. G., Zhang, G. Q., Cao, X. G., Fang, D. Q., & Wang, H. W. (2013). Pygmy and giant dipole resonances by Coulomb excitation using a quantum molecular dynamics model. *Physical Review C—Nuclear Physics*, *87*(1), 014621.

[70] KADoNiS database (2023). Karlsruhe Astrophysical Database of Nucleosynthesis in Stars. https://www.kadonis.org/

[71] Praena, J., Martín-Hernández, G. & García López, J. (2023). Production and measurement of stellar neutron spectrum at 30 keV. *arXiv preprint arXiv: 2301.11266*.

[72] Marganiec, J., Dillmann, I., Pardo, C. D., Käppeler, F., Reifarth, R., Gallino, R., ... & Grabmayr, P. (2009). Neutron capture cross sections of $^{74}$Ge, $^{76}$Ge, and $^{75}$As at 25 keV. *Physical Review C—Nuclear Physics*, *79*(6), 065802.

[73] Dillmann, I., Heil, M., Käppeler, F., Rauscher, T., & Thielemann, F. K. (2006). Experimental (n, γ) cross sections of the p-process nuclei $^{74}$Se and $^{84}$Sr. *Physical Review C—Nuclear Physics*, *73*(1), 015803.

# References

[74] Beer, H., Walter, G., & Käppeler, F. (1992). Measurement of the $^{76}$Se(n, γ) capture cross section and phenomenological s-process studies-The weak component. *Astrophysical Journal*, *389*, 784-790.

[75] Dillmann, I., Heil, M., Käppeler, F., Faestermann, T., Knie, K., Korschinek, G., ... & Rauscher, T. (2008). First measurements of the total and partial stellar cross section to the s-process branching-point $^{79}$Se. *arXiv preprint arXiv:0806.2063*.

[76] Wisshak, K., Voss, F., Theis, C., Käppeler, F., Guber, K., Kazakov, L., ... & Reffo, G. (1996). Stellar neutron capture cross sections of the tin isotopes. *Physical Review C*, *54*(3), 1451.

[77] Koehler, P. E., Harvey, J. A., Winters, R. R., Guber, K. H., & Spencer, R. R. (2001). High-resolution neutron capture and transmission measurements for $^{116,120}$Sn, and their stellar neutron-capture cross sections at s-process temperatures. *Physical Review C*, *64*(6), 065802.

[78] Käppeler, F., Schanz, W., Wisshak, K., & Reffo, G. (1993). The s-process between A= 120 and 124 -Signature of neutron density and temperature in red giants. *Astrophysical Journal*, *410*(1), 370-386.

[79] Wisshak, K., Voss, F., Käppeler, F., & Reffo, G. (1992). Neutron capture in $^{122,123,124}$Te: Critical test for s process studies. *Physical Review C*, *45*(5), 2470.

[80] Reifarth, R., Heil, M., Käppeler, F., Voss, F., Wisshak, K., Becvář, F., ... & Nagai, Y. (2002). Stellar neutron capture cross sections of $^{128,129,130}$Xe. *Physical Review C*, *66*(6), 064603.

[81] Beer, H. (1991). Capture cross section measurements of krypton and xenon isotopes and the fundamental parameters of the s-process. *Astrophysical Journal*, *375*, 823-832.

[82] Käppeler, F., Toukan, K. A., Schumann, M., & Mengoni, A. (1996). Neutron capture cross sections of the cerium isotopes for s-and p-process studies. *Physical Review C*, *53*(3), 1397.

[83] Best, J., Stoll, H., Arlandini, C., Jaag, S., Käppeler, F., Wisshak, K., ... & Rauscher, T. (2001). s-process branchings at $^{151}$Sm, $^{154}$Eu, and $^{163}$Dy. *Physical Review C*, *64*(1), 015801.

[84] Jaag, S., & Käppeler, F. (1995). Stellar (n,γ) cross section of the unstable isotope $^{155}$Eu. *Physical Review C*, *51*(6), 3465.

[85] Wisshak, K., Voss, F., Käppeler, F., Guber, K., Kazakov, L., Kornilov, N., ... & Reffo, G. (1995). Stellar neutron capture cross sections of the Gd isotopes. *Physical Review C*, *52*(5), 2762.

[86] Wisshak, K., Voss, F., Käppeler, F., & Kazakov, L. (1998). Stellar Neutron Capture Cross Sections of the Yb Isotopes. Technical report FZKA-6194, Forschungszentrum Karlsruhe.

[87] Wisshak, K., Voss, F., Arlandini, C., Käppeler, F., & Kazakov, L. (2000). Stellar neutron capture cross sections of the Yb isotopes. *Physical Review C*, *61*(6), 065801.

[88] Marganiec, J., Dillmann, I., Pardo, C. D., Käppeler, F., & Walter, S. (2008, July). First experimental (n, γ) cross sections of heavy p-process nuclei. In *Proc. 10th Symp. Nuclei in the Cosmos*.

[89] Beer, H. & Macklin, R.L. (1985). $^{198,199,200,201,202,204}$Hg(n, γ) cross sections and the termination of s-process nucleosynthesis. *Physical Review C*, *32*(3), 738.

[90] Djerboua, Y., Musacchio-González, E., Mastinu, P., & Amrani, N. (2023). Systematics of Maxwellian-averaged neutron capture cross-sections (MACS) at 30keV. *International Journal of Modern Physics E*, *32*(11), 2350056.

[91] Broeders, C. H. M., & Konobeyev, A. Y. (2006). Semi-empirical systematics of (n, p) reaction cross-section at 14.5, 20, and 30 MeV. *Nuclear Physics A*, *780*(3-4), 130-145.

**Abstract**

This study presents the derivation of a formula for the calculation of Maxwellian Averaged neutron capture Cross Sections (MACS) at 30 keV. Utilizing this derived formula, we establish a linear correlation between the logarithm of MACS at 30 keV divided by $A^{1.4}$ and $(N-Z)^2/A^2$ of the target nucleus. The calculated MACS values, obtained from this correlation, exhibit satisfactory agreement with experimental data, indicating the useful of this new systematic law for analyzing experimental data. Furthermore, this systematic law facilitates the estimation of MACS for neighboring isotopes where experimental data are limited or unavailable.

**Keywords:** formula; neutron capture; MACS; 30 keV; experimental data; systematic law

**Résumé**

Cette étude présente la dérivation d'une formule pour le calcul des sections efficaces de capture de neutrons moyennes maxwelliennes (MACS) à 30 keV. En utilisant cette formule dérivée, nous établissons une corrélation linéaire entre le logarithme de MACS à 30 keV divisé par $A^{1.4}$ et $(N-Z)^2/A^2$ du noyau cible. Les valeurs de MACS calculées, obtenues à partir de cette corrélation, présentent un accord satisfaisant avec les données expérimentales, indiquant l'utilité de cette nouvelle loi systématique pour l'analyse des données expérimentales. De plus, cette loi systématique facilite l'estimation des MACS pour les isotopes voisins lorsque les données expérimentales sont limitées ou indisponibles.

**Mots-clés :** formule ; capture de neutrons ; MACS ; 30 keV ; données expérimentales; loi systématique

**ملخص**

تقدم هذه الدراسة اشتقاق صيغة لحساب المقاطع العرضية لالتقاط النيوترونات المتوسطة ماكسويلية (MACS) عند 30 كيلو إلكترون فولت. باستخدام هذه الصيغة المشتقة، أنشأنا علاقة خطية بين لوغاريتم MACS عند 30 كيلو فولت مقسومًا على $A^{1.4}$ و $(N-Z)^2/A^2$ للنواة المستهدفة. تظهر قيم MACS المحسوبة، التي تم الحصول عليها من هذا الارتباط، اتفاقًا مرضيًا مع البيانات التجريبية، مما يشير إلى فائدة هذا القانون المنهجي الجديد لتحليل البيانات التجريبية. علاوة على ذلك، يسهل هذا القانون المنهجي تقدير MACS للنظائر المجاورة حيث تكون البيانات التجريبية محدودة أو غير متوفرة.

**الكلمات المفتاحية:** الصيغة؛ التقاط النيوترونات؛ MACS؛ 30 كيلو إلكترون فولت؛ بيانات تجريبية؛ قانون منهجي